Journal of Medicinal Chemistry

Article

Discovery of Potent Small Molecule SIRT6 Activators: Structure-Activity Relationship and Anti-pancreatic Ductal Adenocarcinoma Activity

Xiuli Chen, Weining Sun, Shen-Zhen Huang, Hailin Zhang,
Guifeng Lin, Hui Li, Jingxin Qiao, Linli LI, and Shengyong Yang

J. Med. Chem., **Just Accepted Manuscript** • DOI: 10.1021/acs.jmedchem.0c01183 • Publication Date (Web): 12 Aug 2020

is published by the American Chemical Society. 1155 Sixteenth Street N.W., Washington, DC 20036

Discovery of Potent Small Molecule SIRT6 Activators: Structure-Activity Relationship and Anti-pancreatic Ductal Adenocarcinoma Activity

Xiuli Chen[†,‡], Weining Sun[§,‡], Shenzhen Huang[†,‡], Hailin Zhang[†], Guifeng Lin[†], Hui Li[†], Jingxin Qiao[†], Linli Li[§], and Shengyong Yang[†,*]

[†]State Key Laboratory of Biotherapy and Cancer Center, West China Hospital, Sichuan University, Chengdu, Sichuan 610041, P.R. China

[§]Key Laboratory of Drug Targeting and Drug Delivery System of Ministry of Education, West China School of Pharmacy, Sichuan University, Chengdu, Sichuan 610041, P.R. China

[‡] These authors contributed equally to this work.

*To whom correspondence should be addressed. Shengyong Yang, State Key Laboratory of Biotherapy and Cancer Center, West China Hospital, Sichuan University, Chengdu, Sichuan 610041, China. E-mail: yangsy@scu.edu.cn.

KEYWORDS: SIRT6, deacetylation, small molecule activator, anti-pancreatic cancer activity

ABSTRACT

SIRT6 activation is thought to be a promising target for the treatment of many diseases, particularly cancer. Herein, we report the discovery of a series of new small molecule SIRT6 activators. Structure-activity relationship analyses led to the identification of the most potent compound, 2-(1-benzofuran-2-yl)-*N*-(diphenylmethyl) quinolone-4-carboxamide (**12q**), which showed an $EC_{1.5}$ value of 0.58 ± 0.12 μM and an EC_{50} value of 5.35 ± 0.69 μM against SIRT6-dependent peptide deacetylation in Fluor de Lys assay. It exhibited weak or no activity against other HDAC family members as well as 415 kinases, indicating a good selectivity for SIRT6. **12q** significantly inhibited the proliferation and migration of pancreatic ductal adenocarcinoma (PDAC) cells *in vitro*. It also markedly suppressed the tumor growth in a PDAC tumor xenograft model. This compound showed attractive pharmacokinetic properties. Overall, **12q** could be a good lead compound for the treatment of PDAC, and it is worthy of further study.

1. INTRODUCTION

Sirtuins are NAD^+-dependent protein lysine deacetylases that participate in the regulation of many physiological processes, such as the cell cycle, metabolism, stress responses, and aging processes in prokaryotic and eukaryotic species.[1-3] There are seven mammalian sirtuins, SIRT1-SIRT7, and they differ in their subcellular localization and in the substrate proteins they deacetylate.[4, 5] Among these sirtuin family members, of particular importance is SIRT6. The basic functions of SIRT6 include hydrolyzing long-chain acylated substrates, and catalyzing the deacetylation of N^{ε}-acetyl-lysines 9, 18, and 56 of histone H3 (H3K9ac, H3K18ac, and H3K56ac, respectively), which have been associated with many physiological and pathological phenotypes.[6-14] The functional activation of SIRT6 might play an important role in prolonging lifespan and intervening related diseases.[15, 16] A recent study demonstrated that SIRT6 is responsible for the more efficient DNA double-strand break repair in long-lived species, and increased SIRT6 activity corresponds to longer lifespans.[17] Numerous investigations have also shown that SIRT6 is involved in various diseases, such as neurodegenerative diseases,[18, 19] diabetes,[20] cardiovascular diseases,[21, 22] and cancers.[23-28] Notably, SIRT6 has been demonstrated to function as a tumor-suppressor gene in some cancers, implying that SIRT6 activation may have potential value in the treatment of these cancers.[13, 29, 30] For example, SIRT6 was found to be critical for the suppression of pancreatic ductal adenocarcinoma (PDAC), one of the most lethal malignancies.[27] SIRT6 inactivation promotes PDAC progression and metastasis through the upregulation of Lin28b, a negative regulator of let-7 microRNA. Knocking out the SIRT6 gene results in histone hyperacetylation and c-Myc recruitment at the Lin28b promoter, and pronounced induction of Lin28b and downstream let-7 target genes, including IGF2BP1 and IGF2BP3.[27] In contrast,

SIRT6 activation might suppress PDAC progression and reduce metastasis formation via the down regulation of Lin28b.[27] SIRT6 activation is thus thought to be a promising target in PDAC treatment.

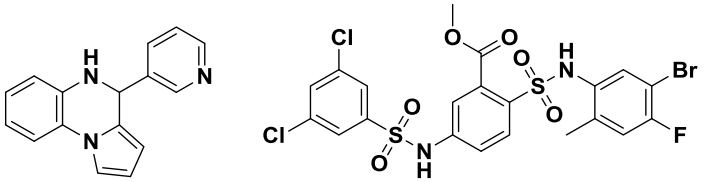

UBCS039 **MDL-800**

Figure 1. Reported synthetic SIRT6 activators.

You *et al* reported the first synthetic SIRT6 activator, a pyrrolo[1,2-a]quinoxaline derivative (**UBCS039**, Figure 1), which binds at a distal region of the fatty-acyl substrate site and "*C* site" of SIRT6.[31, 32] This compound showed an EC_{50} value of 38 μM against SIRT6.[31] Recently, Huang *et al* disclosed a new potent SIRT6 activator with cell activity, methyl 2-(*N*-(5-bromo-4-fluoro-2-methylphenyl)sulfamoyl)-5-(3,5-dichlorophenyl sulfonamido)benzoate (**MDL-800**, Figure 1), which displayed an EC_{50} value of 10.3 μM against SIRT6.[33] **MDL-800** exhibited considerable activity in decreasing H3K9ac and H3K56ac levels in human hepatocellular carcinoma (HCC) cells.[33] Obviously, the potency of these compounds is still not enough from the perspective of a good drug candidate. Therefore, more potent and selective SIRT6 activators with new skeletons are needed.

To discover new SIRT6 activators, we performed a virtual screening against various commercial chemical databases, which led to the discovery of several hit compounds. Structural optimization to the most active hit compound was then carried out, and this process offered a number of SIRT6 activators. The most potent activator was subjected to further studies including assessment of its molecular level biological activities, selectivity, and *in vitro* and *in vivo* anti-PDAC activities.

2. RESULTS AND DISCUSSION

2.1 Discovery of Hit Compounds with the Aid of Molecular Docking-Based Virtual Screening

To obtain new activators of SIRT6, molecular docking was adopted to screen commercial chemical databases including Specs, ChemDiv, Selleck, and MedChemExpress, as well as an in-house database. Here, the crystal structure of the SIRT6-**UBCS039** (PDB entry 5MF6) complex was used, and GOLD was adopted for molecular docking.[31] The SIRT6-specific acyl channel pocket was defined as the active site; this active site was very similar to the allosteric site of SIRT6 identified later by Huang *et al*[33] and was also found to accommodate SIRT6 modulators of the quercetin compound family[32]. GoldScore[34] and ID-Score[35] were utilized to estimate the strength of interactions between the compound and the protein receptor. The final ranking order of compounds was based on the consensus score of GoldScore and ID-Score.[36, 37] All the calculations were carried out with Discovery Studio (DS) 3.1 (Accelrys Inc., San Diego, CA, USA).[38]

From the top ranked compounds, 40 compounds (**Hit01**-**Hit40**) were selected and purchased for biochemical assays. We first tested the activity of each of these compounds at a fixed concentration of 100 μM by the Fluor de Lys (FDL) assay using a fluorogenic AMC-myristoyl peptide substrate (Ac-EALPKK(Myr)-AMC).[31, 33, 39] In this assay, four compounds (**Hit05**, **Hit07**, **Hit11**, and **Hit20**) showed clear activating effects at 100 μM against SIRT6 (Figure 2A and 2B, and Supplementary Table S1). We then measured the $EC_{1.5}$ values of these compounds; $EC_{1.5}$ is defined as the concentration of a compound at which the compound is able to increase the enzymatic activity by 50%.[40, 41] The calculated $EC_{1.5}$ values are 118.20 ± 1.33 μM, 109.80 ± 1.09 μM, 227.50 ± 1.31 μM, and 27.14 ± 1.18 μM for **Hit05**, **Hit07**, **Hit11**, and **Hit20**,

respectively (Figure 2B and 2C). Structural optimization and structure-activity relationship analyses were then carried out on the most active compound, **Hit20**.

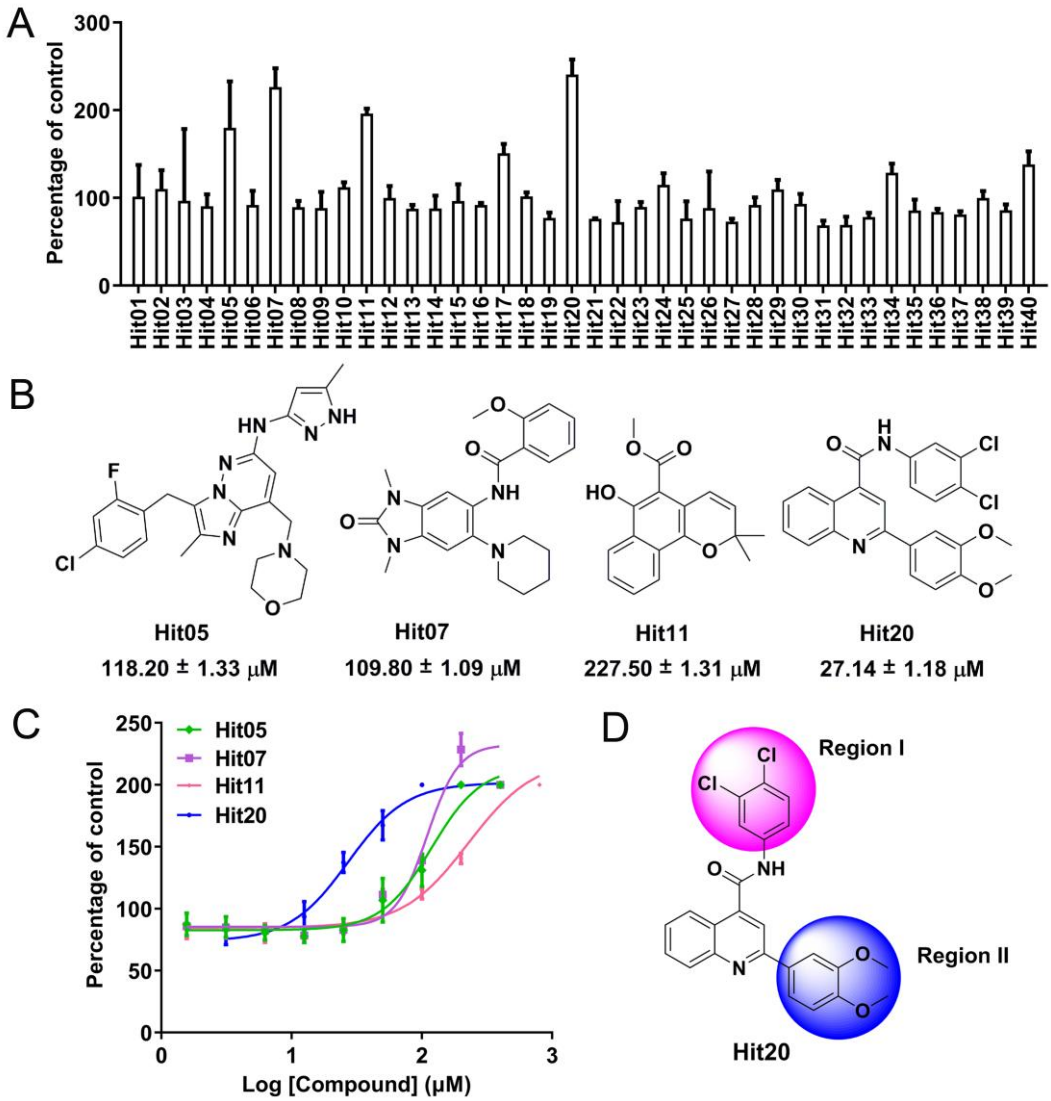

Figure 2. *In vitro* SIRT6 enzymatic activity assay for the screened compounds. **A**) Activation of SIRT6-dependent peptide demyristoylation by 40 selected compounds at 100 μM, determined with Ac-EALPKK(Myr)-AMC by the FDL assay. **B**) Chemical structures of hit compounds **Hit05**, **Hit07**, **Hit11**, and **Hit20**. **C**) Dose-dependent demyristoylation activities of SIRT6 by 4 hit compounds, determined with Ac-EALPKK(Myr)-AMC by the FDL assay. Data are presented as the mean ± s.d., $n = 3$ wells, from three independent experiments. **D**) Target regions for the structural optimization and SAR analyses.

2.2 Structural Optimization and Structure-Activity Relationship (SAR) Analyses of Hit20

To facilitate the structural optimization, molecular docking was used again to predict the binding mode of **Hit20** with SIRT6. As shown in Figure S1, **Hit20** binds to the specific acyl channel pocket of SIRT6, a similar binding site of **UBCS039** and **MDL-801**.[31-33] A face-to-face π-π interaction between the benzene ring of the quinoline scaffold and the phenyl ring of PHE86, and a σ-π interaction between the amino group of ALA-7 and the benzene ring of 3,4-dichlorobenzene are formed. We also noticed that there is some space not completely occupied around 3,4-dichlorobenzene group (the 4-position carboxamide substituent on the quinoline, region I) and 3,4-dimethoxybenzene group (2-position on the quinoline, region II). It is expected that modifications to these two regions, for example adding hydrogen bond donors or receptors, or increasing hydrophobic interaction, might benefit the improvement of bioactivity. Therefore, the subsequent structural optimization will focus on region I and region II (Figure 2D). The SAR analyses are based on the activation potencies of the compounds against SIRT6, which were determined by an FDL assay with peptide Ac-EALPKK(Myr)-AMC as the substrate.

2.2.1 Impact of the 4-Position Carboxamide Substituents (Region I, R^1) on the Quinolone

To examine the influence of 4-position carboxamide substituents (region I, R^1) on the quinolone on the bioactivity, we fixed region II as the original 3,4-dimethoxy phenyl group and varied the group in region I. Here region I groups chosed include phenyl groups with different substituents, as well as other fragments that might help increase hydrogen bonding interaction and/or hydrophobic interaction. Forty quinoline-4-carboxamide derivatives (**PC01-40**) with different R^1 substituents were

purchased from commercial reagent companies. In addition, we also synthesized fifteen new quinoline-4-carboxamide derivatives (**5a-o**). The synthetic routes of **5a-o** are depicted in **Scheme 1**. Condensation reactions of commercially available indolin-2,3-dione (**1**) and 3,4-dimethoxyacetophenone (**2**) in EtOH in the presence of an appropriate amount of KOH aqueous solution generated 2-(3,4-dimethoxyphenyl) quinolone-4-carboxylic acid (**3**) as an intermediate a yield of 76%. Intermediate **3** was then reacted with various substituted anilines to offer final products **5a-o**. The final yields were between 45%-79%.

Scheme 1. Synthesis of compounds **5a-o**.[a]

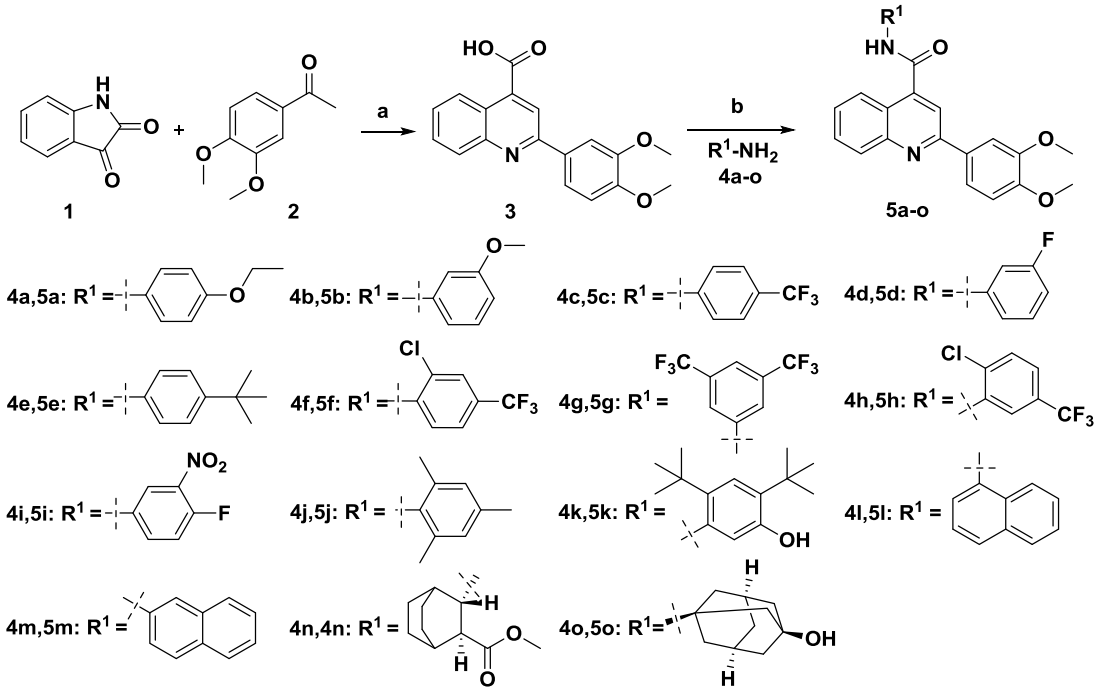

[a] **Reagents and conditions:** a) KOH, EtOH, 85 ℃, 24 h; b) i: $SOCl_2$, 107 °C, 5-6 h; ii: R^1-NH_2, DMAP, DMF, RT, overnight.

The chemical structures and bioactivities of compounds **PC01-40** and **5a-o** are given in Table 1. Among compounds **PC01-24** and **5a-k** containing substituted phenyl groups at the R^1 position, eight compounds (**5a**, **PC12**, **PC14**, **PC17**, **5f-h**, and **5j**)

displayed activation effects of >150% at 20 μM. $EC_{1.5}$ values of these compounds are 10.28 ± 2.38 μM, 5.97 ± 1.99 μM, 19.02 ± 1.14 μM, 5.61 ± 1.24 μM, 7.53 ± 1.31 μM, 6.38 ± 1.98 μM, 2.84 ± 0.37 μM, and 4.77 ± 1.81 μM, respectively. For compounds **PC25-40** and **5l-o**, which contain a naphthalene ring, benzyl moiety, polyunsaturated ring or heterocycle with larger substituents, six compounds (**5l**, **PC25-26**, and **PC28-30**) showed activation potencies of >150% at 20 μM. The $EC_{1.5}$ values of these compounds are 7.44 ± 2.08 μM, 5.97 ± 1.98 μM, 6.47 ± 4.40 μM, 7.78 ± 1.60 μM, 19.53 ± 1.35 μM, and 8.14 ± 1.59 μM, respectively. Of all the fifty-five compounds, **5h**, which contains a 2-chloro-5-(trifluoromethyl) phenyl group, is the most active one in terms of the $EC_{1.5}$ values. We then fixed the R^1 substituent as a 2-chloro-5-(trifluoromethyl) phenyl group in the following optimization step.

Table 1. Chemical Structures and Effect of Compounds **PC01-40** and **5a-o** on SIRT6-dependent Peptide Demyristoylation Activation.

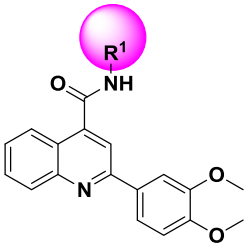

ID	R^1	% Effect @20 μM ($EC_{1.5}$/μM)	ID	R^1	% Effect @20 μM ($EC_{1.5}$/μM)
Hit20	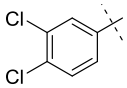	147.60 (27.14 ± 1.18)	**PC01**	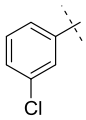	103.89
PC02	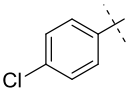	98.69	**PC03**		104.63
PC04	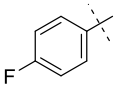	104.33	**PC05**		92.42

PC06	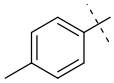	98.32	**PC07**	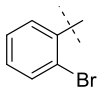	128.49
PC08	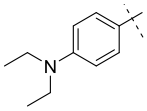	83.32	**PC09**	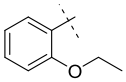	95.21
PC10	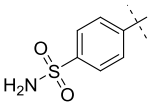	131.49	**PC11**	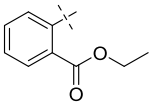	117.76
5a	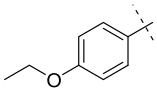	165.72 (10.28 ± 2.38)	**5b**	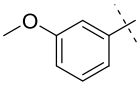	114.98
5c	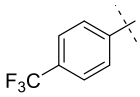	141.68	**5d**	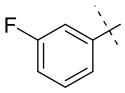	142.38
5e	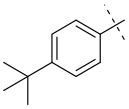	124.45	**PC12**	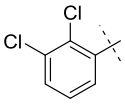	223.94 (5.97 ± 1.99)
PC13	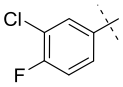	107.90	**PC14**	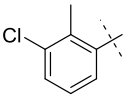	198.91 (19.02 ± 1.14)
PC15	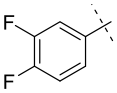	101.37	**PC16**	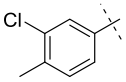	116.66
PC17	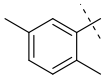	313.43 (5.61 ± 1.24)	**PC18**	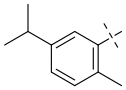	131.17
5f	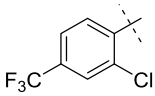	181.36 (7.53 ± 1.31)	**5g**	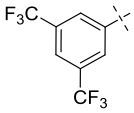	249.98 (6.38 ± 1.98)
5h	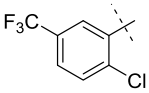	364.62 (2.84 ± 0.37)	**PC19**	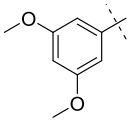	102.9
5i	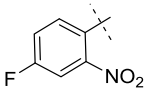	65.66	**PC20**	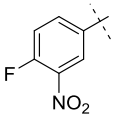	96.94
PC21	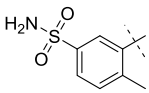	95.52	**PC22**	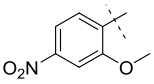	100.97
PC23	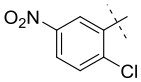	98.19	**PC24**	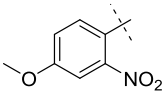	87.18

5j	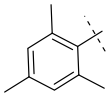	284.13 (4.77 ±1.81)	**5k**	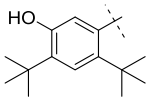	88.61
5l		326.96 (7.44 ±2.08)	**5m**	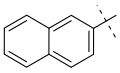	139.32
PC25	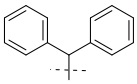	276.15 (5.97 ±1.98)	**PC26**	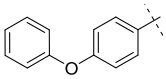	239.45 (6.47 ±4.40)
PC27	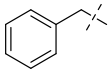	107.49	**PC28**	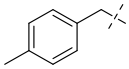	225.36 (7.78 ±1.60)
PC29	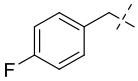	168.5 (19.53 ±1.35)	**PC30**	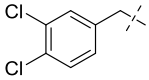	259.94 (8.14 ±1.59)
PC31	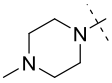	105.48	**PC32**		124.23
PC33		99.04	**5n**	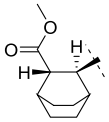	127.6
5o	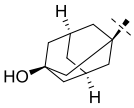	86.13	**PC34**	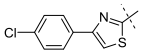	90.98
PC35	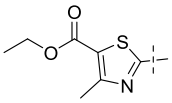	90.3	**PC36**	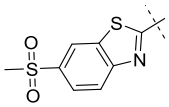	83.37
PC37	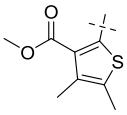	101.43	**PC38**	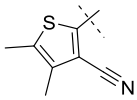	95.12
PC39	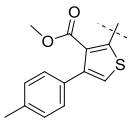	82.90	**PC40**	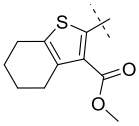	95.22

2.2.2 Effect of the 2-Position (Region II, R^2) on the Quinolone

To explore the effect of the substituent at the 2-position (region II, R^2) of quinolone, we installed 5-member ring, 6-member ring, or benzoheterocycles in region II (R^2) and fixed region I as the optimal 2-chloro-5-(trifluoromethyl)phenyl group. We purchased two quinolone-4-carboxamide derivatives with different

substituents at R^2 (**PC41-42**) and synthesized thirteen new quinolone-4-carboxamide derivatives (**8a-m**). **Scheme 2** illustrates the synthetic routes of compounds **8a-m**. Similar to before, the condensation reactions between indolin-2,3-dione (**1**) and various substituted acetophenones (**6a-m**) in EtOH in the presence of an appropriate amount of KOH aqueous solution generated 2-substituted quinolinone-4-carboxylic acids (**7a-m**) as intermediates. The final products (**8a-m**) were then obtained from the reactions of **7a-m** with commercially available 2-chloro-5-(trifluoromethyl) aniline.

Scheme 2. Synthesis of compounds **8a-m**.[a]

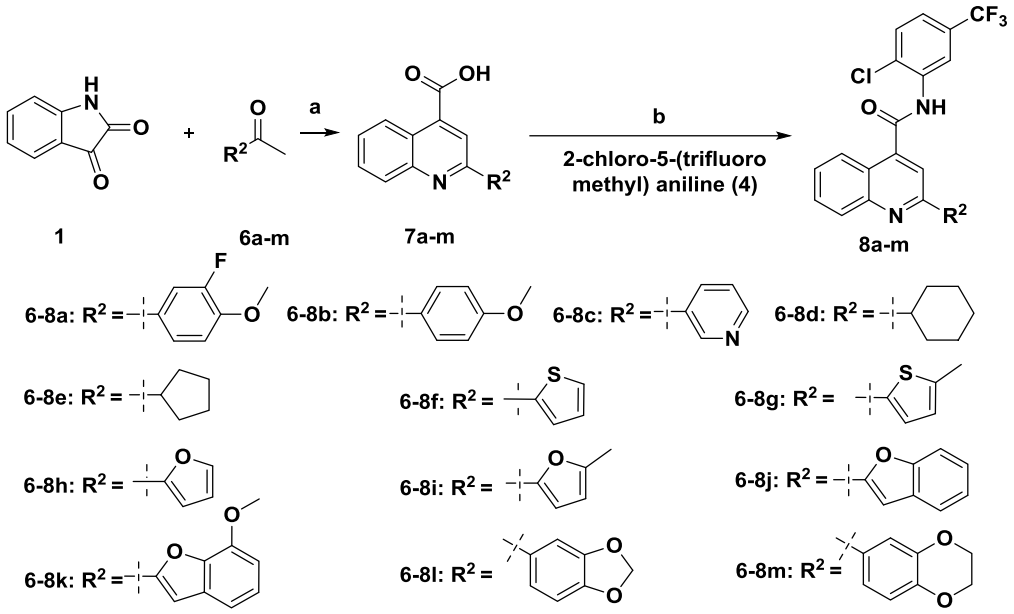

[a] **Reagents and conditions:** a) KOH, EtOH, 85 ℃, 24 h; b) i: $SOCl_2$, 107 °C, 5-6 h; ii: 2-chloro-5-(trifluoromethyl)aniline, DMAP, DMF, RT, overnight.

The chemical structures and bioactivities of compounds **PC41-42** and **8a-m** are shown in Table 2. Compounds **PC41-42** and **8a**, containing a different substituted phenyl groups, did not activate SIRT6. Compound **8b** with 4-methoxyphenyl did activate SIRT6 with an $EC_{1.5}$ value of 20.72 ± 3.01 μM. Compounds **8d** and **8e**, bearing saturated five- or six-membered rings, also did not activate SIRT6. In addition,

compounds **8f** and **8g**, which contain a (substituted) thiophene at the R^2 position, did not show obvious activity against SIRT6 at 20 μM. Interestingly, compounds **8h-m**, bearing a (substituted) furan, or a benzo oxygen-containing heterocycle, displayed obvious activation effects, and **8j** is the most active one with an $EC_{1.5}$ value of 0.85 ± 0.36 μM .

Table 2. Chemical Structures and Effect of Compounds **PC41-42** and **8a-m** on SIRT6-dependent Peptide Demyristoylation Activation.

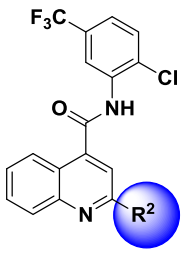

ID	R^2	% Effect @20 μM ($EC_{1.5}$/μM)	ID	R^2	% Effect @20 μM ($EC_{1.5}$/μM)
5h	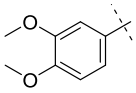	364.62 (2.84 ± 0.37)	**PC41**	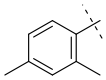	92.33
PC42	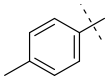	108.96	**8a**	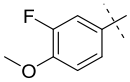	91.20
8b	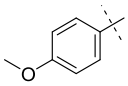	163.4 (20.72 ± 3.01)	**8c**		85.57
8d		82.43	**8e**		76.38
8f		130.20	**8g**	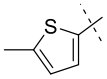	141.05
8h		140.80	**8i**	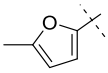	184.00 (18.61 ± 1.61)
8j	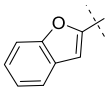	762.05 (0.85 ± 0.36)	**8k**	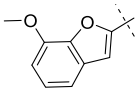	321.32 (5.96 ± 1.36)

8l	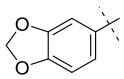	228.42 (14.86 ± 1.47)	**8m**	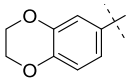	158.86 (29.39 ± 5.37)

2.2.3 Re-optimization of the 4-Position (Region I, R^3) on the Quinolone

In the preceding SAR studies, we determined an optimal moiety (benzofuranyl group) for region II with region I fixed as 2-chloro-5-(trifluoromethyl)phenyl, which was also determined through optimization. To examine whether 2-chloro-5-(trifluoromethyl)phenyl is still optimal when region II is fixed as a benzofuranyl moiety, we synthesized seventeen compounds with different substituents at the 4-position (region I, R^3) of the quinolone (**12a-q**). Compounds **12a-q** were prepared following the route outlined in **Scheme 3**, which is very similar to that in **Scheme 1**.

Scheme 3. Synthesis of compounds **12a-q**.[a]

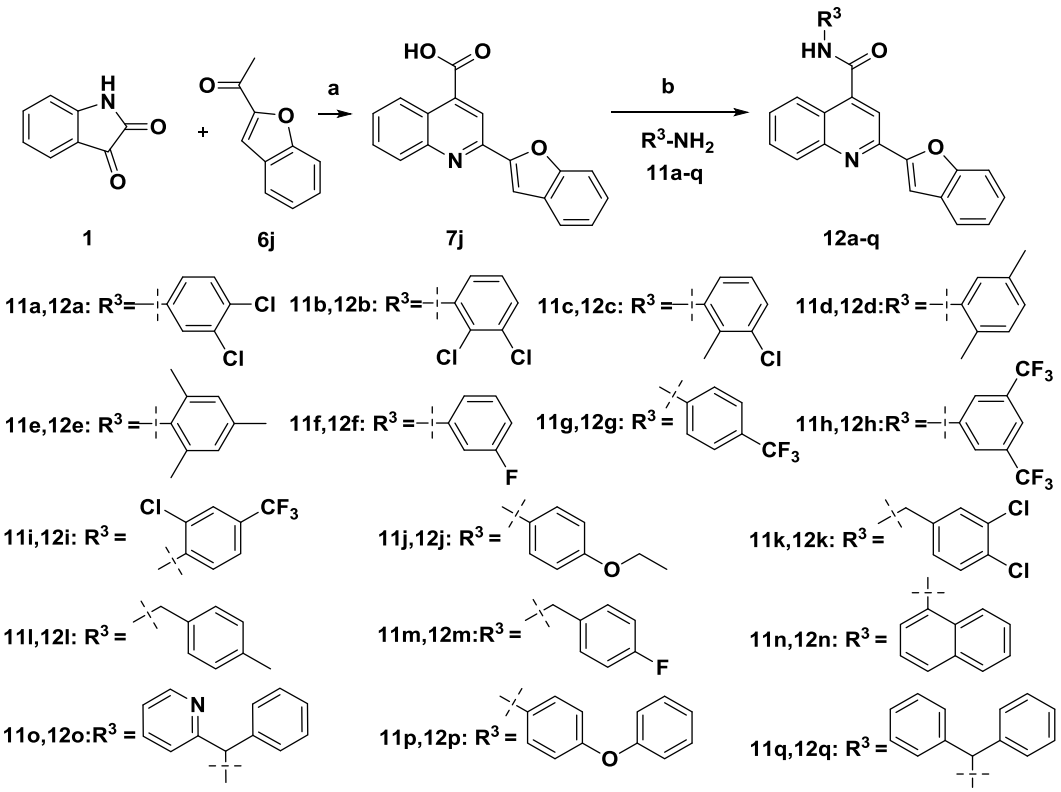

[a] **Reagents and conditions:** a) KOH, EtOH, 85 °C, 24 h; b) R^3-NH_2, HATU, HOBt, DMAP, 50 °C, overnight.

Bioactivities of compounds **12a-q** are shown in Table 3. All the compounds showed obvious activities against SIRT6 at 20 μM. Compound **12q**, which contains a diphenylmethane group in region I, exhibited more potent activity than **8j**. The $EC_{1.5}$ value of compound **12q** is 0.72 ±0.25 μM, which is 38-fold more potent than **Hit20**.

Table 3. Chemical Structure and Effect of Compounds **12a-q** on SIRT6-dependent Peptide Demyristoylation Activation.

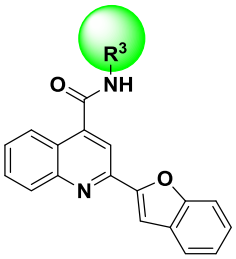

ID	R^3	% Effect @ 20μM ($EC_{1.5}$ /μM)	ID	R^3	% Effect @ 20μM ($EC_{1.5}$ /μM)
8j	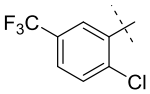	762.05 (0.85 ±0.36)	**12a**	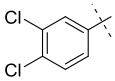	108.95
12b	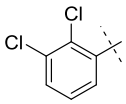	163.48 (20.72 ±5.76)	**12c**	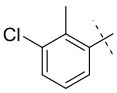	204.83 (9.01 ±3.51)
12d	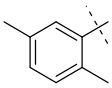	348.60 (3.47 ±0.97)	**12e**	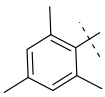	314.93 (3.71 ±1.67)
12f	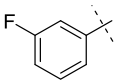	215.60 (4.86 ±1.76)	**12g**	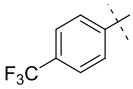	334.64 (5.17 ±1.90)
12h	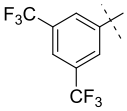	429.78 (3.11 ±1.99)	**12i**	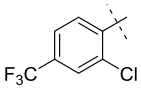	287.42 (4.96 ±2.20)
12j	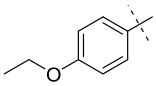	109.27	**12k**	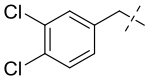	313.96 (5.91 ±1.53)

12l	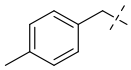	208.02 (14.50 ±3.94)	**12m**	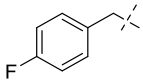	481.51 (2.19 ±1.02)
12n	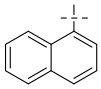	119.23	**12o**	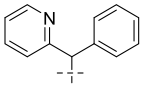	321.40 (7.59 ±0.99)
12p	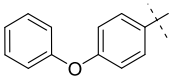	118.25	**12q**	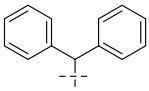	1229.81 (0.72 ±0.25)

2.3 Bioactivity Validation of Compound 12q by Various Biochemical and Biophysical Assays

To further validate the bioactivity of **12q** *in vitro*, various biochemical and biophysical assays were performed, including FDL assays but with different substrate peptides, differential scanning fluorimetry (DSF) assays, isothermal titration calorimetry (ITC) assays, and surface plasmon resonance (SPR) assays. **MDL-800** was used as a reference compound because it is the most potent SIRT6 activator reported so far.

2.3.1 FDL Assay with Different Substrate Peptides

As indicated before,[42] deacetylation is one of most important functions of SIRT6. We thus validated the influence of **12q** on the deacetylation activity of SIRT6. To this end, the FDL assay was used again, and acetyl peptide substrate (Ac-RYQK(Ac)-AMC) was used.[43] As shown in Figure 3A, compound **12q** dramatically enhanced SIRT6 deacetylation activity with an $EC_{1.5}$ value of 0.58 ±0.12 μM, which is comparable to that of demyristoylation activity (0.72 ± 0.25 μM, Table 3). Dose-dependent curves of **12q** against SIRT6 deacetylation and demyristoylation are displayed in Figure 3A and 3B, respectively. And the calculated EC_{50} values of **12q** are 5.35 ± 0.69 μM and 8.91 ± 1.81 μM for SIRT6 deacetylation and demyristoylation, respectively. Collectively, **12q** is able to enhance both the

deacetylation activity and demyristoylation activity of SIRT6. Though the positive control **MDL-800** showed excellent SIRT6-dependant deacetylation activity, it could not enhance the demyristoylation activity of SIRT6 (Figure 3B), which is consistent with Huang's result.[33]

One may notice that different peptides were used in deacetylation (Ac-RYQK(Ac)-AMC) and demyristoylation (Ac-EALPKK(Myr)-AMC) assays. To examine possible influence of different peptides in FdL assays, we tested the activity of **12q** with Ac-RYQK(Myr)-AMC as the substrate. The measured $EC_{1.5}$ and EC_{50} values are 0.49 ± 0.11 μM and 5.49 ± 0.57 μM (Figure S2), respectively, which are comparable to the corresponding values in the cases of Ac-RYQK(Ac)-AMC and Ac-EALPKK(Myr)-AMC. All the results indicate that different peptide substrates have no significant impact on the bioactivity.

2.3.2 DSF Assay

The bioactivity of **12q** was then validated by the DSF assay, which is a spectroscopic technique used to identify the thermal stability of a protein.[44] In this assay, the recombinant human protein SIRT6 was used as the target protein. The thermal stability of SIRT6 in the presence or absence of small molecule ligands was measured. The melting temperature (T_m) values of SIRT6 are 41.18 ± 0.10 °C and 42.19 ± 0.10 °C treated with DMSO and **12q** at a concentration of 20 μM, respectively, indicating a ΔT_m value of 1.01 °C (Figure 3C). At the same concentration, **MDL-800** displayed a ΔT_m value of 0.85 °C.

2.3.3 ITC and SPR Assays

ITC and SPR assays were adopted to measure the binding affinity of **12q** with SIRT6. In the ITC assay, **12q** showed an equilibrium dissociation constant (K_d) of 8.85 ± 1.89 μM (Figure 3D). The measured thermodynamic binding parameters are

14.33 ± 5.60 kcal mol^{-1}, 71.20 cal mol^{-1} K^{-1}, -6.90 ± 5.60 kcal mol^{-1} and -21.23 kcal mol^{-1} for Δ*H*, Δ*S*, Δ*G*, and -TΔ*S*, respectively. The stoichiometry factor (N) is 0.31 ± 0.098. In the SPR assay, compound **12q** displayed an equilibrium dissociation constant (Kd) of 5.52 μM (Figure 3E). **MDL-800** showed a K_d of 9.51 μM in the same assay (Figure S3).

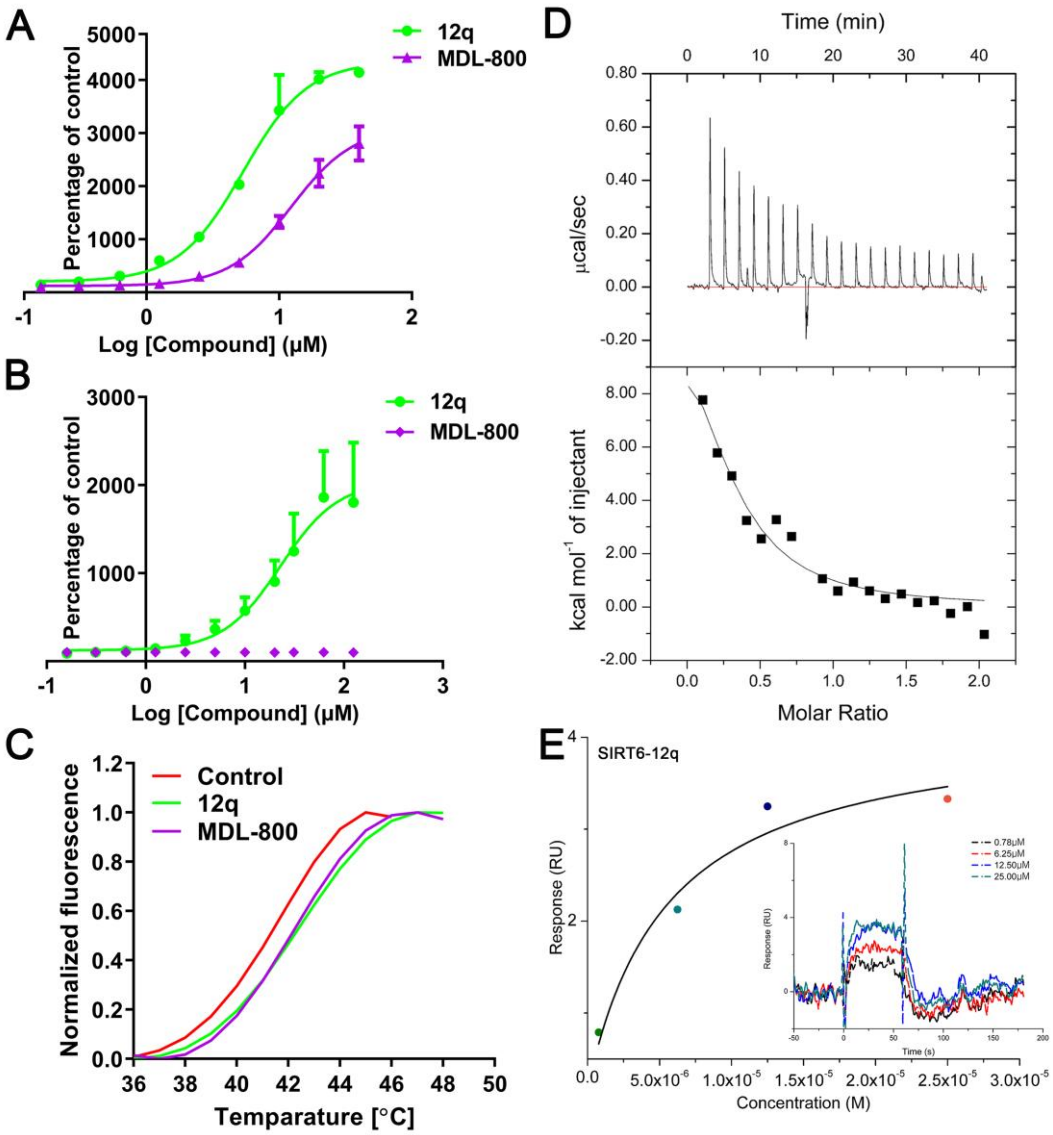

Figure 3. Bioactivities of **12q** against SIRT6 by various biochemical and biophysical assays. **A**, **B**) Dose-activity curves of SIRT6-dependant deacetylation and demyristoylation of **12q**, determined with acetyl substrate peptide Ac-RYQK(Ac)-AMC and myristoyl substrate peptide Ac-EALPKK(Myr)-AMC. Data are presented as the mean ± s.d., *n*= 3 wells, from three independent experiments. **C**) Changes in the thermodynamic stability of SIRT6 after the binding

of **12q** or **MDL-800**. **D**) ITC binding curves for SIRT6 and **12q**. **E**) Representative SIRT6 binding curves and fit steady-state evaluation for **12q** using SPR.

2.3.4 High Performance Liquid Chromatography (HPLC) Assay

The HPLC assay was applied to test the SIRT6-dependant deacetylase activity of **12q**. Here, both peptide substrates Ac-RYQK(Ac)-AMC and Ac-EALPKK(Myr)-AMC were used. The results showed that **12q** could enhance the SIRT6-dependant deacetylation and demyristoylation activities (Figure S4).

2.4 Selectivity of 12q

To test the selectivity of **12q**, we measured the half maximal inhibitory concentration (IC_{50}) values of **12q** against other HDAC family members, including SIRT1-3, SIRT5, and HDAC1-11; SIRT4 and SIRT7 are not involved because they are not available for us at present. As shown in Table 4, **12q** potently activated SIRT6 but showed no activity toward SIRT2, SIRT3, SIRT5, and HDAC1-11 at concentrations up to 200 μM. Although **12q** exhibited activity against SIRT1, the potency is almost 300 folds lower than that against SIRT6. We further tested the activity of **12q** against a panel of 415 recombinant human kinases, and **12q** showed no activity or very weak activity against these kinases (Table S2). These results indicated that **12q** is a selective activator of SIRT6 and is not a Pan Assay Interference Compound (PAIN).

Table 4. Activities of **12q** against HDAC Family Members.

Target	IC_{50} μM	Target	IC_{50} μM
SIRT1	171.20 ± 14.98	HDAC4	>200
SIRT2	>200	HDAC5	>200

SIRT3	>200	HDAC6	>200
SIRT5	>200	HDAC7	>200
SIRT6	0.58 ± 0.12 ($EC_{1.5}$) [a]	HDAC8	>200
HDAC1	>200	HDAC9	>200
HDAC2	>200	HDAC10	>200
HDAC3	>200	HDAC11	>200

[a]The activity of **12q** against SIRT6 was determined by the FDL assay with acetyl substrate peptide Ac-RYQK(Ac)-AMC.

2.5 Predicted Binding Mode of 12q

Because we failed to obtain a crystal structure of the **12q**-SIRT6 complex, molecular docking was used again to predict the binding mode of **12q** and SIRT6. Figure 4 presents a predicted binding mode of **12q** with SIRT6. **12q** occupies the allosteric pocket, which is very similar to that of **UBCS039**[31] and **MDL-801**[33] (also see Figure S5, a superposition of three complex structures). The oxygen atom of the carboxamide of **12q** forms one hydrogen bond with the amide group in the side chain of ASN4. The *N*-benzhydryl group of **12q** fit perfectly in the allosteric pocket via hydrophobic interactions with residues TYR5, VAL70, PHE82, PRO62, and PRO80. The benzofuran forms hydrophobic interactions with LYS160 and MET157. Two face-to-face π−π and one σ−π interactions are formed. One of the π−π interactions is between the benzene ring of the *N*-benzhydryl group and the benzene ring of residue PHE82, and the other π−π interaction is between the benzene ring of the quinoline and the benzene ring of residue PHE86. The σ-π interaction is between the benzene ring in the benzofuran group and the amino group in THR156 (Figure 4). These interactions well explain the high potency of **12q**.

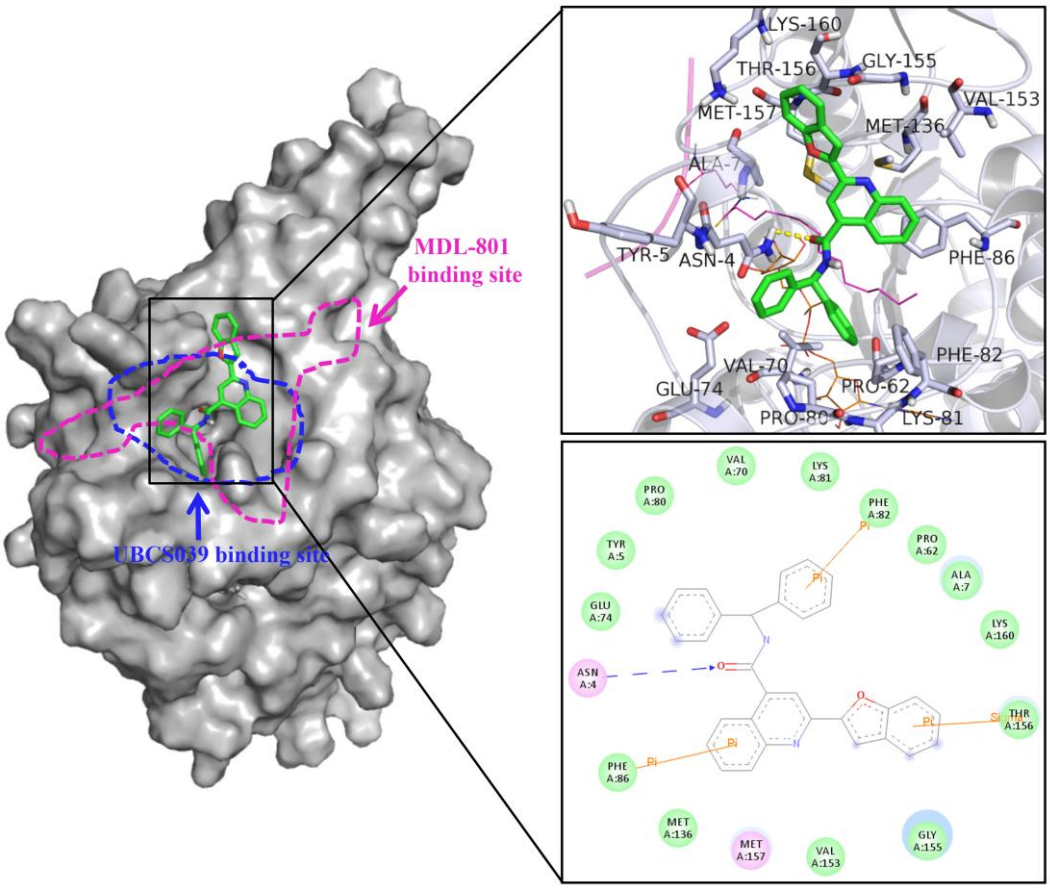

Figure 4. Predicted binding mode of **12q** with SIRT6 (the SIRT6 structure was taken from PDB entry 5Y2F). **12q** (green), ADPR (apricot), H3K9-Myr (magenta) are show in the "zoomed-in" image.

2.6 *In Vitro* Anti-PDAC Activities of Compound 12q

2.6.1 Anti-viability and Anti-proliferation Activities of 12q Against PDAC Cells

The MTT assay was used to measure the anti-viability activity of **12q** against PDAC cells. Four human PDAC cell lines, PANC-1, BXPC-3, MIAPaCa-2, and AsPC-1, were chosen for this study. As shown in Figure 5A, **12q** exhibited anti-viability activity against all the tested cell lines in a dose-dependent manner, with IC_{50} values of 4.13 ± 0.15 μM, 8.27 ± 1.08 μM, 7.10 ± 1.85 μM, and 9.66 ± 1.13 μM, against PANC-1, BXPC-3, MIAPaCa-2, and AsPC-1, respectively. In this assay, **MDL-800** also showed activity but with relatively weak potency (IC_{50} values of 35.19 ± 1.21 μM, 57.96 ± 1.11 μM, 55.65 ± 1.03 μM, 50.51 ± 1.01 μM for PANC-1,

BXPC-3, MIAPaCa-2, and AsPC-1, respectively) (Figure 5B). To examine the tumor-specificity effect, we tested the anti-viability activity of **12q** against eight cell lines of other tumor types, including two liver cancer cell lines (HEPG2 and BEL7402), one thyroid cancer cell line (OCUT-2C), one ovarian cancer cell line (SKOV-3), one colon cancer cell line (SW620), and three lung cancer cell lines (H526, H1975, and NCl-H446). Although **12q** displayed some activities against these tumor cell lines, the potencies are weaker compared with those of PDAC cell lines (Table S3), indicating a certain degree of selectivity for PDAC cells.

The colony formation assay was performed to investigate the anti-proliferation activity of **12q** against PDAC cells. As shown in Figure 5C and Figure S6A, compound **12q** could inhibit the colony formation of PANC-1, BXPC-3, MIAPaCa-2, and AsPC-1 cells in a dose dependent-manner. The anti-proliferation activity of **12q** was further confirmed by an EdU incorporation assay (Figure 5D and Figure S6B).

2.6.2 Cell Cycle Arrest and Apoptosis Induction Ability of 12q Against PDAC Cells

Flow cytometry was adopted to detect cell cycle arrest and apoptotic cells upon treatment with **12q**. The results showed that compound **12q** caused a dose-dependent increase in the percentages of PANC-1 and BXPC-3 cells in the G2 phase (Figure S7), indicating that **12q** could cause PDAC cell arrest in the G2 phase. **12q** treatment also increased Annexin V^+ populations in a concentration-dependent manner, implying that **12q** could induce apoptosis in PANC-1 and BXPC-3 cells (Figure S8).

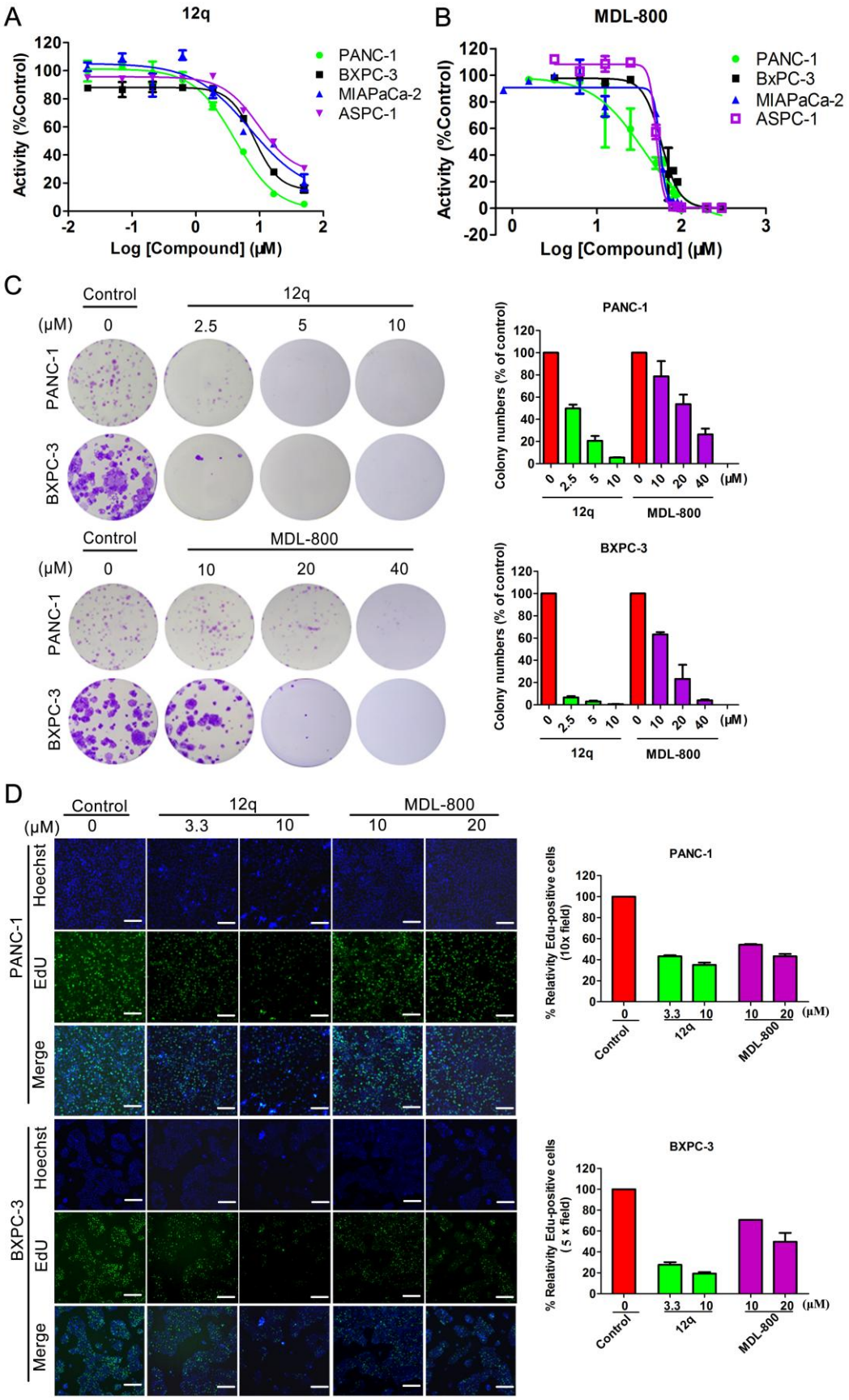

Figure 5. Antiproliferative activities of **12q** against pancreatic cancer cells *in vitro*. **A**, **B**) Cells were treated with the indicated agents for 72 h, and cell viability was measured by an MTT assay.

Every experiment was carried out in triplicate. **C**) Cells were incubated with various concentrations of the indicated agents for 18 days (BXPC-3) or 14 days (PANC-1). Then, the cells were stained with crystal violet and quantified. **D**) The fluorescence microscopic appearance of EdU and Hoechst on BXPC-3 and PANC-1 cells after treatment with the indicated agents for 24 h. EdU-positive cells were quantified in 10 fields. Scale bars, 100 μm.

2.6.3 Anti-migration Ability of 12q

A wound-healing assay was used to evaluate the anti-migration ability of **12q** *in vitro*. Four human PDAC cell lines, PANC-1, BXPC-3, MIAPaCa-2, and AsPC-1, were used for this experiment. As shown in Figure 6A and Figure S9, **12q** significantly inhibited the migration of PDAC cells in a time- and dose-dependent manner, with migration inhibition rates reaching approximately 87.8%, 70.0%, 57.2%, and 55.4% in the presence of 10 μmol/L **12q** at 24 h, respectively.

2.7 Bioactivities of 12q in Intact Cells

The cellular thermal shift assay (CETSA) was first used to investigate whether **12q** could bind to the SIRT6 protein in intact cells. As shown in Figure 6B, **12q** treatment efficiently protected SIRT6 protein from temperature-dependent degradation in PANC-1 and BXPC-3 cells, indicating that **12q** is able to bind to SIRT6. Western blot was used to examine the effect of **12q** on the acetylation status of H3K9ac, H3K18ac, and H3K56ac in intact cells; H3K9, H3K18, and H3K56 are the typical substrates of SIRT6. As shown in Figure 6C, **12q** decreased the levels of H3K9ac, H3K18ac, and H3K56ac in PANC-1 and BXPC-3 cells in a dose-dependent manner. **MDL-800** showed the same effect.

We further investigated the influence of **12q** on the Lin28b / let-7 signal pathway in PDAC cells. As indicated before, it has been reported that SIRT6 functional loss accelerates PDAC progression and metastasis via upregulation of Lin28b, and c-Myc recruitment. As displayed in Figure 6C, **12q** treatment decreased the expression of

Lin28b and c-Myc.

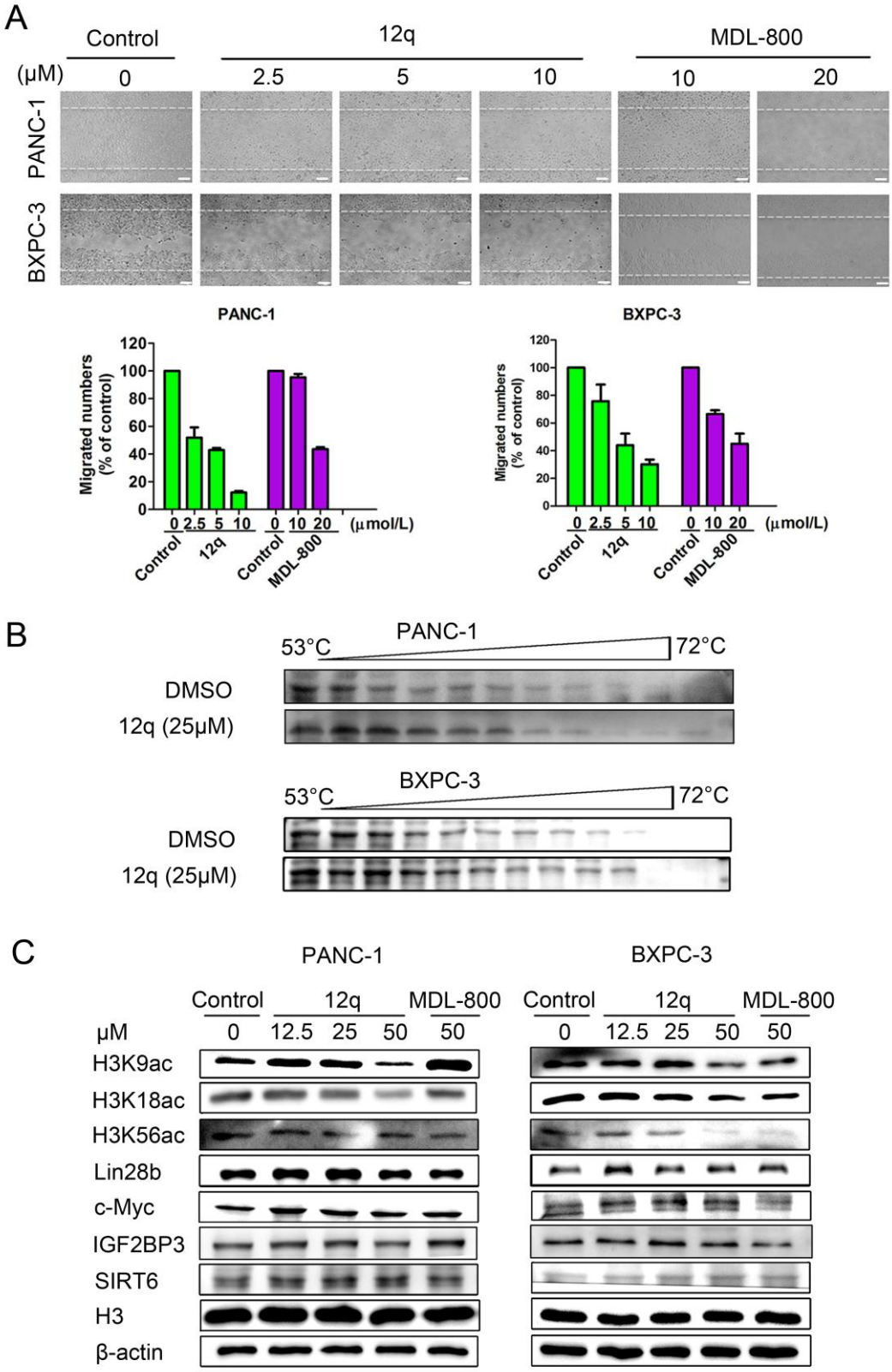

Figure 6. Anti-migration ability of **12q** and its bioactivities in intact cells. **A**) Anti-migration activity of **12q** against pancreatic cancer cells *in vitro*. BXPC-3 or PANC-1 cells were treated with various concentrations of the indicated agents. Scale bars, 100 μm. **B**) Western blot analysis of SIRT6 and its substrates H3K9ac, H3K18ac, and H3K56ac, and Lin28b, c-Myc, and IGF2BP3 protein expression in PANC-1 and BXPC-3 cells treated with the indicated doses of **12q** and **MDL-800** for 72 h. **C**) A cellular thermal shift assay (CETSA) was implemented in intact cells exposed to **12q** (25 μM).

2.8 *In Vivo* Effects of 12q on Subcutaneous PANC-1 Tumor Xenograft

To evaluate the antitumor activity of **12q** *in vivo*, we used the human pancreatic tumor xenograft model of PANC-1. BALB/c female nude mice were orally administered 100 or 150 mg/kg/d of **12q** for 30 days. **MDL-800** (150 mg/kg/d) was used as a positive control. In all the treated group, tumor growth was slowed by **12q** in a dose-dependent manner, and a tumor inhibition rate of 90.25% at a dose of 150 mg/kg was observed (Figure 7A and 7B). No significant weight loss or toxicity were observed compared with the control group (Figures S10 and S11). **MDL-800** also showed considerable antitumor potency with a tumor inhibition rate of 78.03% at a dose of 150 mg/kg/d.

To elucidate the mechanism of **12q**-mediated antitumor efficacy *in vivo*, we conducted immunohistochemistry (IHC) analysis in the PANC-1 tumor model. As depicted in Figure 7C, **12q** potently inhibited the expression of Lin28b and c-Myc and led to a substantial decrease in tumor cell proliferation (Ki-67-positive cells) compared with the control group in the PANC-1 tumor model. The level of H3K9ac was lower in the **12q**-treated groups than in the vehicle group. These results revealed that **12q** may suppress PDAC xenograft tumor growth *in vivo* by activating the deacetylase activity of SIRT6.

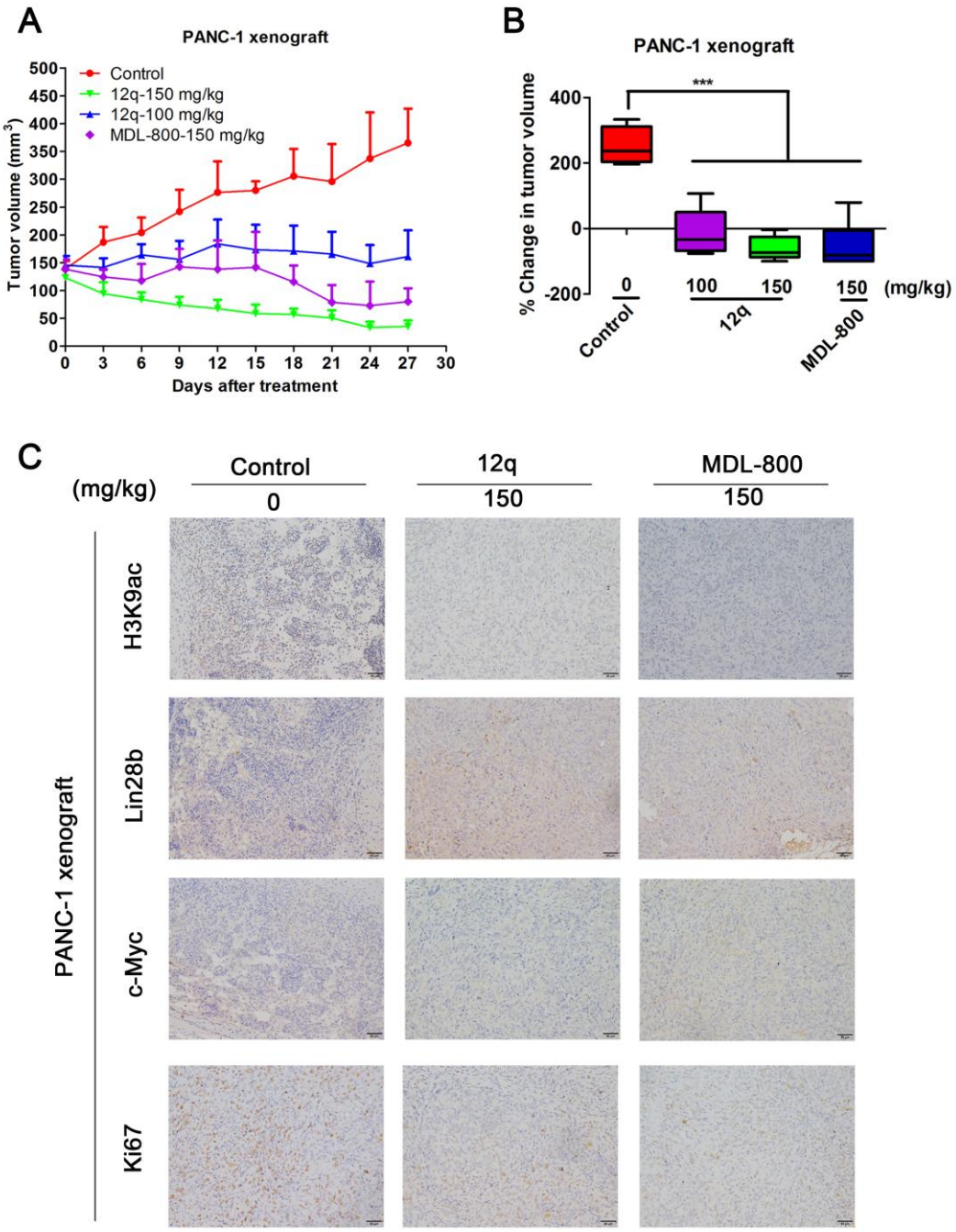

Figure 7. Antitumor efficacy of **12q** *in vivo*. **A**) Mice bearing PANC-1 tumor xenografts were treated with agents at the indicated dose or vehicle control alone over the designated treatment schedule once tumors reached the determined size (n=6). Points, mean tumor volume; bars, SD. **B**) Quantitative analysis of tumor volumes on the final study day. ***P < 0.001. **C**) Tumor tissue from PANC-1 xenografts treated with vehicle control, **12q** (150 mg/kg), or reference agents at the dose mentioned above were evaluated by IHC. Scale bars, 50 μm.

2.9 Preliminary Pharmacokinetic Properties of 12q

The preliminary pharmacokinetic (PK) properties of compound **12q** were determined by oral administration to male Sprague-Dawley rats. The pharmacokinetic parameters of **12q** at a dose of 10 mg/kg are summarized in Table 5. The area under the concentration-time curve ($AUC_{(0-\infty)}$) is 755.57 h·ng/mL. The maximum plasma concentration (C_{max}) is 98.45 ng/mL. The bioavailability (F) and half-life ($T_{1/2}$) are 4% and 7.52 h, respectively.

Table 5. *In vitro* Pharmacokinetic Profiles of Compound **12q**.

Pharmacokinetic parameter	10 mg/kg p.o. [a]	2 mg/kg i.v. [a]
CL (L/h/kg)	-	0.6 ± 0.08
Vss (L/kg)	-	1112.8 ± 322.84
$T_{1/2}$ (h)	7.52 ± 1.44	9.06 ± 0.21
T_{max} (h)	2.00 ± 0.00	0.08 ± 0.00
C_{max} (ng/mL)	98.45 ± 3.62	5123.70 ± 905.5
$AUC_{(0-t)}$ (h·ng/mL)	704.67 ± 80.47	3326.13 ± 476.4
$AUC_{(0-\infty)}$ (h·ng/mL)	755.57 ± 80.74	3381.49 ± 468.48
F (%)	4.24 ± 0.48	-

[a] Expressed as Mean ± SD, n = 3

3. CONCLUSIONS

In this investigation, we identified a potent SIRT6 activator, 2-(1-benzofuran-2-yl)-*N*-(diphenylmethyl)quinolone-4-carboxamide (**12q**), through virtual screening, chemical synthesis, and SAR analyses. This compound showed $EC_{1.5}$ value of 0.58 ± 0.12 μM (EC_{50} = 5.35 ± 0.69 μM) and 0.72 ± 0.25 μM (EC_{50} = 8.91 ± 1.81 μM) against SIRT6 in the FDL assays with acetyl peptide and myristoyl peptide substrates, respectively. The bioactivity of **12q** was further validated by DSF, SPR, and ITC assays. In target selectivity assays, **12q** displayed excellent selectivity for SIRT6 against other tested SIRT family members and HDACs. In various *in vitro*

assays including MTT, colony formation, flow cytometry, and wound-healing assays, **12q** exhibited considerable anti-PDAC activities. In the subcutaneous PANC-1 tumor xenograft model, **12q** showed potent anti-tumor activity. **12q** also exhibited fairly good pharmacokinetic (PK) properties. Overall, **12q** could be a promising lead compound for the treatment of pancreatic cancer and is worthy of further in-depth studies.

4. MATERIALS AND METHODS

4.1 Virtual Screening Based on Molecular Docking

In this study, molecular docking was performed using GOLD (Genetic Optimization of Ligand Docking) 5.0.[34, 45] X-ray crystal structures of SIRT6 in complex with **UBCS039** (PDB entry 5MF6) and **MDL-801** (PDB entry 5Y2F) were used in the docking studies.[33] The Discovery Studio 3.1 (Accelrys, Inc. USA) software package was adopted to prepare the protein structure, including adding hydrogen atoms to the protein, removing water molecules, and assigning the force field (here, the CHARMm force field was adopted). The binding site was defined as a sphere containing residues within 10 Å of the ligand, an area large enough to cover the ligand-binding region. Compound libraries, including Specs, ChemDiv, Selleck, MedChemExpress, and an in-house database, were filtered by SMARTS-PAINS and Other Bad Groups as reported[38], and used for the virtual screening in this investigation.

4.2 Chemistry Methods

Starting materials, reagents, and solvents used in the experiments were purchased from commercial vendors unless otherwise noted, and they were analytically pure or chemically pure. Anhydrous solvents were either dried by distillation under reduced pressure or purchased from J&K Scientific. All reactions were monitored by

thin-layer chromatography (TLC) carried out on Merck silica gel plates (0.25 mm thick, 60F254) and visualization was achieved by UV light. ^{1}H NMR (proton nuclear magnetic resonance) spectra, ^{13}C NMR (carbon-13 nuclear magnetic resonance) spectra and HRMS/ESI-MS (high resolution mass spectrometry/ electrospray ionization mass spectrometry) were used for characterization. ^{1}H NMR and ^{13}C NMR spectra were recorded with Bruker Avance III 400 MHz spectrometers, and chemical shifts are reported in parts per million (δ, ppm) relative to the internal reference tetramethylsilane (Me_4Si, TMS). NMR spectra were acquired in $CDCl_3$ or DMSO-d_6. ^{1}H NMR data are reported as follows: chemical shift [multiplicity (s = singlet, d = doublet, t = triplet, q = quartet, dd = doublet of doublets, dt = doublet of triplets, m = multiplet, br s = broad singlet), *J*= coupling constant(s) (Hz), integration]. ^{13}C NMR data are reported as follows: chemical shift [multiplicity (if not singlet), assignment (Cq = fully substituted carbon)]. HRMS and low-resolution ESI−MS date were recorded on an Agilent 1200- G6410A mass spectrometer using an electrospray ionization (ESI) source. All the final compounds were purified to >95% purity, as determined by high-performance liquid chromatography (HPLC). HPLC analyses were performed on a Waters e2695 HPLC system with a Symmetry® C18 column (4.6 mm × 250 mm, 5 μm). The binary solvent system (A/B) was as follows: methanol (A) and water (B), A/B= 80/20. The flow rate was 1.0 mL/min. The yields of all reactions refer to the purified products. All final compounds were routinely characterized by melting points (Mp), as determined on a Mel-Temp melting point apparatus, and the reported values are uncorrected.

General Procedure for the Preparation of the 2-Substituted Quinolinone-4-carboxylic Acid (3,7a-m).[46, 47]

Example: 2-(3,4-Dimethoxyphenyl)quinolone-4-carboxylic acid (3): The synthetic pathway for the preparation of compound **3** is depicted in Scheme 1. Indolin-2,3-dione (**1**, 1.47 g, 20.0 mmol), 3,4-dimethoxyacetophenone (**2**, 2.16 g, 24.0 mmol) and KOH (1.68 g, 60 mmol)) in ethanol (35 mL) were added to a 100 mL round bottom flask with stirring. The resulting mixture was heated to reflux at 85 ℃ for 48 h. After the reaction was complete, the solvent was removed under reduced pressure, and the residue was dissolved in water and washed twice with ethyl acetate. The aqueous layer was concentrated and adjusted to pH = 2 with concentrated HCl. The solid was separated by filtration, washed with water until neutral, dried, and purified by flash column chromatography over silica gel eluting with ethyl acetate and petroleum ether to obtain 2-(3,4-dimethoxyphenyl)quinolone-4-carboxylic acid (**3**) as a yellow solid in 76% yield. ^{1}H NMR (400 MHz, DMSO-d_6) δ 13.95 (s, 1H), 8.59 (dd, J = 8.5, 1.3 Hz, 1H), 8.43 (s, 1H), 8.17-8.09 (m, 1H), 7.91 (d, J = 2.1 Hz, 1H), 7.87 (dd, J = 8.4, 2.1 Hz, 1H), 7.83 (ddd, J = 8.4, 6.8, 1.5 Hz, 1H), 7.66 (ddd, J = 8.3, 6.8, 1.3 Hz, 1H), 7.14 (d, J = 8.4 Hz, 1H), 3.92 (s, 3H), 3.86 (s, 3H). ^{13}C NMR (101 MHz, DMSO) δ 168.2, 156.0, 151.2, 149.6, 148.8, 138.1, 131.0, 130.5, 130.0, 127.7, 125.8, 123.6, 120.8, 119.2, 112.2, 110.7, 56.1. MS m/z (ESI): 310.11 $[M+H]^+$.

General Procedure for the Preparation of the 2-Substituted Quinoline-4-carboxamide Derivatives (5a-o, 8a-m, and 12a-q).[48, 49]

Example:

***N*-[2-Chloro-5-(trifluoromethyl)phenyl]-2-(3,4-dimethoxyphenyl)quinolone-4-carboxamide (5h):** The synthetic pathways for the preparation of compounds **5a-o** and **8a-m** are depicted in Scheme 1 and Scheme 2. In a 25 mL round bottom flask, intermediate compound **3** (155 mg, 0.5 mmol) was dissolved in $POCl_3$ (6 mL) and heated to 107 ℃ for 4-5 h.[50] The progress of the reaction was monitored by TLC, and

the reaction solution concentrated by rotary evaporation after completion of the reaction. The obtained acid chloride compound was dissolved in dry DMF, and 3-amino-4-chlorobenzotrifluoride (4, 117 mg, 0.6 mmol) and DMAP (12.2 mg, 0.1 mmol) were added, and the reaction was allowed to stand overnight. After completion of the reaction, the reaction mixture was diluted with water and extracted with ethyl acetate. The organic layer was washed three times with saturated aqueous NaCl, and dried over anhydrous Na_2SO_4. *N*-[2-chloro-5-(trifluoromethyl)phenyl]-2-(3,4-dimethoxyphenyl)quinolinone-4-carbo xamide (**5h**), yield 79%. Mp 209.7-210.6 ℃. ^{1}H NMR (400 MHz,DMSO-d_6) δ 10.84 (s, 1H), 8.41 (s, 1H),8.30 (d, J = 2.2 Hz, 1H), 8.26 (d, J = 8.2 Hz, 1H), 8.15 (d, J = 8.4 Hz, 1H), 7.97 (d, J = 1.8 Hz, 1H), 7.94 (dd, J = 8.4, 2.5 Hz, 1H), 7.88-7.81 (m, 2H), 7.71 (dd, J = 7.6, 2.1 Hz, 1H),7.65 (t, J = 7.7Hz, 1H), 7.17 (d, J = 8.5 Hz, 1H), 3.94 (s, 3H), 3.87 (s, 3H).^{13}CNMR (101 MHz, DMSO) δ 166.6, 155.9, 151.2, 149.6, 142.5, 136.1, 133.6, 131.5, 131.2, 130.7, 129.9, 128.8, 128.5, 127.5, 125.6, 125.1, 124.6, 123.4, 122.8, 120.9, 117.4, 112.2, 110.8, 56.2, 56.1. HRMS m/z (ESI) calcd for $C_{25}H_{19}ClF_3N_2O_3$ $[M+H]^+$ 487.1031 found: 487.1027, calcd for $C_{25}H_{18}ClF_3N_2O_3Na$ $[M+Na]^+$ 509.0850 found: 509.0859.

General Procedure for the Preparation of the 2-Substituted Quinoline-4-carboxamide Derivatives (12a-q).

Example:

2-(1-Benzofuran-2-yl)-*N*-[4-(trifluoromethyl)phenyl]quinolone-4-carboxamide (12g): The synthetic pathway for the preparation of compounds (**12a-q**) is depicted in Scheme 3. Similar to compound **3**, 2-(1-benzofuran-2-yl)quinolone-4-carboxylic acid (**7j**) was obtained from the condensation of indolin-2,3-dione (**1**) and 1-(benzofuran-2-yl)ethan-1-one (**6j**). The reaction of compound **7j** (289 mg, 1 mmol)

with the proper commercially available substituted amine (for example **11g**, 4-(trifluoromethyl)aniline, 161 mg, 1 mmol) was stirred overnight at 50 °C with HATU (380 mg, 1 mmol) and HOBt (135 mg, 1 mmol) as condensation agents and DMAP (12 mg, 0.1 mmol) as a base. This two-step reaction provides compound **12g** as a white solid in 35% yield. Mp 294.8-296.1 ℃. ^{1}H NMR (400 MHz, DMSO-d_6) δ 11.26 (s, 1H), 8.42 (s, 1H), 8.19 (dd, J = 16.9, 8.4 Hz, 2H), 8.05 (d, J = 8.4 Hz, 2H), 7.99 (s, 1H), 7.90 (ddd, J = 8.4, 6.8, 1.5 Hz, 1H), 7.82-7.77 (m, 4H), 7.72 (ddd, J = 8.3, 6.9, 1.3 Hz, 1H), 7.49-7.44 (m, 1H), 7.36 (t, J = 7.5 Hz, 1H). ^{13}C NMR (101 MHz, DMSO) δ 165.9, 155.5, 154.6, 148.4, 143.1, 142.8, 131.3, 130.0, 128.7, 128.5, 126.7, 126.2, 125.6, 124.9, 124.6, 124.2, 123.8, 123.5, 122.7, 120.5, 116.9, 112.2, 108.0. HRMS m/z (ESI) calcd for $C_{25}H_{16}F_3N_2O_2$ $[M+H]^+$ 433.1158 found: 433.1166, calcd for $C_{25}H_{15}F_3N_2O_2Na$ $[M+Na]^+$ 455.0978 found: 455.0982.

2-(3,4-Dimethoxyphenyl)-*N*-(4-ethoxyphenyl)quinoline-4-carboxamide (5a): white solid. Yield 60%. Mp 169.3-170.1 ℃. ^{1}H NMR (400 MHz, DMSO-d_6) δ 10.66 (s, 1H), 8.32 (s, 1H), 8.16-8.10 (m, 2H), 7.97 (d, J = 6.9 Hz, 2H), 7.81 (ddd, J = 8.3, 6.9, 1.4 Hz, 1H), 7.77-7.71 (m, 2H), 7.62 (ddd, J = 8.3, 6.8, 1.2 Hz, 1H), 7.18-7.11 (m, 1H), 6.97 (d, J = 9.0 Hz, 2H), 4.03 (q, J = 6.9 Hz, 2H), 3.93 (s, 3H), 3.86 (s, 3H), 1.34 (t, J = 6.9 Hz, 3H).^{13}C NMR (101 MHz, DMSO) δ 165.4, 156.0, 155.5, 151.1, 149.6, 148.3, 143.6, 132.4, 131.3, 130.6, 129.9, 127.3, 125.6, 123.5, 122.0, 116.8, 114.9, 112.2, 110.9, 63.6, 56.2, 56.1, 15.2. HRMS m/z (ESI) calcd for $C_{26}H_{25}N_2O_4$ $[M+H]^+$ 429.1809 found: 429.1813, calcd for $C_{26}H_{24}N_2O_4Na$ $[M+Na]^+$ 451.1628 found: 451.1633.

2-(3,4-Dimethoxyphenyl)-*N*-(3-methoxyphenyl)quinoline-4-carboxamide (5b): White solid. Yield 65%. Mp 171.6-172.9 ℃. ^{1}H NMR (400 MHz, DMSO-d_6) δ 10.79 (s, 1H), 8.33 (s, 1H), 8.12 (dd, J = 11.6, 8.5 Hz, 2H), 7.98-7.95 (m, 2H), 7.84-7.80 (m,

1H), 7.67-7.59 (m, 1H), 7.56-7.52 (m, 1H), 7.39 (d, *J* = 8.2 Hz, 1H), 7.31 (d, *J* = 6.5 Hz, 1H), 7.15 (d, *J* = 8.5 Hz, 1H), 6.76 (dd, *J* = 11.6, 6.5 Hz, 1H), 3.93 (s, 3H), 3.86 (s, 3H), 3.78 (s, 3H).^{13}C NMR (101 MHz, DMSO) δ 166.0, 160.0, 156.0, 151.2, 149.6, 148.3, 143.4, 140.5, 131.2, 130.6, 130.1, 129.9, 127.4, 125.5, 123.3, 120.9, 116.9, 112.7, 112.2, 110.9, 110.1, 106.2, 56.2, 56.1, 55.6.HRMS m/z (ESI) calcd for $C_{25}H_{23}N_2O_4$ $[M+H]^+$415.1652 found: 415.1654, calcd for $C_{25}H_{22}N_2O_4Na$ $[M+Na]^+$ 437.1472 found: 437.1482.

2-(3,4-Dimethoxyphenyl)-*N*-[4-(trifluoromethyl)phenyl]quinoline-4-carboxamide (5c): White solid. Yield 67%. Mp 211.3-212.6 ℃. ^{1}H NMR (400 MHz, DMSO-d_6) δ11.17 (s, 1H), 8.40 (s, 1H), 8.19-8.09 (m, 2H), 8.05 (d, *J* = 8.5 Hz, 2H), 7.98 (dq, *J* = 4.5, 2.1 Hz, 2H), 7.88-7.76 (m, 3H), 7.64 (ddd, *J* = 8.2, 6.9, 1.3 Hz, 1H), 7.15 (d, *J* = 9.0 Hz, 1H), 3.92 (s, 3H), 3.86 (s, 3H). ^{13}C NMR (101 MHz, DMSO) δ 166.4, 156.0, 151.2, 149.6, 148.3, 142.9, 131.1, 130.7, 129.9, 127.5, 126.7, 126.6, 125.4, 124.8, 123.2, 121.0, 120.4, 117.0, 112.2, 110.9, 56.2, 56.1. HRMS m/z (ESI) calcd for $C_{25}H_{20}F_3N_2O_3$ $[M+H]^+$ 453.1421 found: 453.1423, calcd for $C_{25}H_{20}F_3N_2O_3Na$ $[M+Na]^+$ 475.1240 found: 475.1252.

2-(3,4-Dimethoxyphenyl)-*N*-(3-fluorophenyl)quinoline-4-carboxamide (5d): White solid. Yield 63%. Mp 203.9-205.6 ℃. ^{1}H NMR (400 MHz, DMSO-d_6) δ 11.02 (s, 1H), 8.37 (s, 1H), 8.17-8.08 (m, 2H), 8.01-7.95 (m, 2H), 7.86-7.79 (m, 2H), 7.64 (ddd, *J* = 8.2, 6.8, 1.3 Hz, 1H), 7.59-7.54 (m, 1H), 7.50-7.42 (m, 1H), 7.15 (d, *J* = 9.0 Hz, 1H), 7.01 (td, *J* = 8.4, 2.6 Hz, 1H), 3.93 (s, 3H), 3.86 (s, 3H).^{13}C NMR (101 MHz, DMSO) δ 166.2, 156.0, 151.2, 149.6, 148.3, 143.1, 131.2, 131.1, 131.0, 130.7, 129.9, 127.5, 125.4, 123.2, 121.0, 117.0, 116.2, 112.2, 110.9, 56.2, 56.1. HRMS m/z (ESI) calcd for $C_{24}H_{20}FN_2O_3$ $[M+H]^+$ 403.1452 found: 403.1460, calcd for $C_{24}H_{19}FN_2O_3Na$ $[M+Na]^+$ 425.1272 found: 525.1276.

***N*-(4-Tert-butylphenyl)-2-(3,4-dimethoxyphenyl)quinoline-4-carboxamide (5e):** White solid. Yield 61%. Mp 228.4-229.3 ℃. ^{1}H NMR (400 MHz, DMSO-d_6) δ 10.74 (s, 1H), 8.31 (s, 1H), 8.17-8.08 (m, 2H), 7.96 (d, J = 7.3 Hz, 2H), 7.82 (ddd, J = 8.4, 6.9, 1.4 Hz, 1H), 7.75 (d, J = 8.7 Hz, 1H), 7.62 (ddd, J = 8.1, 6.8, 1.3 Hz, 1H), 7.42 (d, J = 8.7 Hz, 2H), 7.14 (d, J = 8.9 Hz, 1H), 3.92 (s, 3H), 3.86 (s, 3H), 1.30 (s, 9H). ^{13}C NMR (101 MHz, DMSO) δ 165.7, 156.0, 151.1, 149.6, 148.3, 147.0, 143.5, 136.8, 131.3, 130.6, 129.9, 127.3, 125.9, 125.5, 123.4, 120.9, 120.2, 116.9, 112.2, 110.9, 56.2, 56.1, 34.6, 31.7. HRMS m/z (ESI) calcd for $C_{28}H_{29}N_2O_3$ $[M+H]^+$ 441.2173 found: 441.2180, calcd for $C_{28}H_{28}N_2O_3Na$ $[M+Na]^+$ 463.1992 found: 463.1995.

***N*-[2-Chloro-4-(trifluoromethyl)phenyl]-2-(3,4-dimethoxyphenyl)quinoline-4-carboxamide (5f):** White solid. Yield 70%. Mp 186.8-187.5 ℃. ^{1}H NMR (400 MHz, DMSO-d_6) δ 10.83 (s, 1H), 8.38 (s, 1H), 8.22 (dd, J = 8.4, 1.3 Hz, 1H), 8.15 (d, J = 8.4 Hz, 2H), 8.04 (d, J = 2.1 Hz, 1H), 7.99-7.92 (m, 2H), 7.90-7.81 (m, 2H), 7.66 (ddd, J = 8.2, 6.9, 1.3 Hz, 1H), 7.17 (d, J = 8.4 Hz, 1H), 3.93 (s, 3H), 3.87 (s, 3H). ^{13}C NMR (101 MHz, DMSO) δ 166.5, 156.0, 151.2, 149.6, 148.3, 142.3, 138.9, 131.2, 130.7, 129.9, 129.3, 128.5, 127.5, 127.3, 125.4, 125.2, 123.4, 120.9, 117.4, 112.3, 110.9, 56.2, 56.1. HRMS m/z (ESI) calcd for $C_{25}H_{19}ClF_3N_2O_3$ $[M+H]^+$ 487.1031 found: 487.1037, calcd for $C_{25}H_{18}ClF_3N_2O_3Na$ $[M+Na]^+$ 509.0850 found: 509.0862.

***N*-[3,5-Bis(trifluoromethyl)phenyl]-2-(3,4-dimethoxyphenyl)quinoline-4-carboxamide (5g).** Off-white solid (yield: 69%). Mp 215.1-216.5 ℃. ^{1}H NMR (400 MHz, DMSO-d_6) δ 11.44 (s, 1H), 8.59-8.50 (m, 2H), 8.46 (s, 1H), 8.18 (dd, J = 15.6, 8.4 Hz, 2H), 7.98-7.95 (m, 2H), 7.91 (s, 1H), 7.88-7.81 (m, 1H), 7.65 (t, J = 7.6 Hz, 1H), 7.16 (d, J = 8.5 Hz, 1H), 3.93 (s, 3H), 3.87 (s, 3H). ^{13}C NMR (101 MHz, DMSO) δ 166.7, 156.0, 151.3, 149.6, 148.4, 142.2, 141.2, 131.5, 131.2, 131.1, 130.8, 129.9, 127.6, 125.5, 125.1, 123.0, 122.3, 121.0, 120.3, 117.5, 117.2, 112.2, 110.9, 56.2, 56.1.

HRMS m/z (ESI) calcd for $C_{26}H_{19}F_6N_2O_3$ $[M+H]^+$ 521.1294 found: 521.1286, calcd for C26H18F6N2O$_3$Na $[M+Na]^+$ 543.1114 found: 543.1125.

2-(3,4-Dimethoxyphenyl)-*N*-(4-fluoro-2-nitrophenyl)quinoline-4-carboxamide(5i): Alight yellow solid. Yield 45%. Mp 203.9-205.3 ℃. ^{1}H NMR (400 MHz, DMSO-d_6) δ 11.23 (s, 1H), 8.35 (s, 1H), 8.23 (dd, J = 8.4, 1.4 Hz, 1H), 8.19-8.13 (m, 1H), 8.04 (dd, J = 8.5, 2.9 Hz, 1H), 7.97 (d, J = 2.1 Hz, 1H), 7.92 (dd, J = 8.4, 2.1 Hz, 1H), 7.88-7.72 (m, 3H), 7.67 (ddd, J = 8.2, 6.8, 1.3 Hz, 1H), 7.18 (d, J = 8.5 Hz, 1H), 3.94 (s, 3H), 3.87 (s, 3H). ^{13}C NMR (101 MHz, DMSO) δ 166.1, 160.3, 157.9, 155.9, 151.3, 149.6, 148.4, 144.6, 141.9, 131.1, 130.9, 130.0, 127.6, 125.4, 123.3, 121.8, 121.6, 120.9, 117.2, 113.1, 112.3, 110.8, 56.2, 56.1. HRMS m/z (ESI) calcd for $C_{24}H_{19}FN_3O_5$ $[M+H]^+$ 448.1303 found: 448.1309, calcd for $C_{24}H_{18}FN_3O_5Na$ $[M+Na]^+$ 470.1123 found: 470.1134.

2-(3,4-Dimethoxyphenyl)-*N*-(2,4,6-trimethylphenyl)quinoline-4-carboxamide (5j): Off-white solid. Yield 59%. Mp 222.8-223.9 ℃. ^{1}H NMR (400 MHz, DMSO-d_6) δ 10.12 (s, 1H), 8.26 (d, J = 6.7 Hz, 2H), 8.15 (d, J = 8.4 Hz, 1H), 7.97 (s, 1H), 7.91 (d, J = 8.4 Hz, 1H), 7.83 (t, J = 7.7 Hz, 1H), 7.66 (t, J = 7.7 Hz, 1H), 7.18 (d, J = 8.4 Hz, 1H), 6.99 (s, 2H), 3.93 (s, 3H), 3.87 (s, 3H), 2.33 (s, 6H), 2.28 (s, 3H). ^{13}C NMR (101 MHz, DMSO) δ 165.9, 156.1, 151.2, 149.6, 148.4, 143.3, 136.5, 135.6, 132.3, 131.4, 130.7, 129.9, 129.0, 127.4, 125.6, 123.7, 121.0, 117.0, 112.3, 110.9, 56.2, 56.1, 21.0, 18.7. HRMS m/z (ESI) calcd for $C_{27}H_{27}N_2O_3$ $[M+H]^+$ 427.2016 found: 427.2021, calcd for $C_{27}H_{26}N_2O_3Na$ $[M+Na]^+$ 449.1836 found: 449.1845.

***N*-(2,4-Di-tert-butyl-5-hydroxyphenyl)-2-(3,4-dimethoxyphenyl)quinoline-4-carboxamide (5k):** White solid. Yield 58%. Mp 254.1-255.5 ℃. ^{1}H NMR (400 MHz, DMSO-d_6) δ 10.08 (s, 1H), 9.33 (s, 1H), 8.27 (dd, J = 8.4, 1.4 Hz, 1H), 8.16 (d, J = 8.1 Hz, 2H), 7.92 (d, J = 2.1 Hz, 1H), 7.88-7.81 (m, 2H), 7.67 (ddd, J = 8.3, 6.8, 1.3

Hz, 1H), 7.25 (s, 1H), 7.20 (d, *J* = 8.5 Hz, 1H), 6.79 (s, 1H), 3.93 (s, 3H), 3.87 (s, 3H), 1.40 (br s, 18H). ^{13}C NMR (101 MHz, DMSO) δ 166.9, 155.9, 154.3, 151.2, 149.6, 148.5, 143.1, 136.7, 134.4, 133.7, 131.4, 130.7, 130.0, 127.3, 125.5, 125.0, 123.6, 120.7, 119.4, 116.7, 112.4, 110.7, 56.1, 34.9, 31.7, 29.8. HRMS m/z (ESI) calcd for $C_{32}H_{37}N_2O_4$ $[M+H]^+$ 513.2748 found: 513.2754, calcd for $C_{32}H_{36}N_2O_4Na$ $[M+Na]^+$ 535.2567 found: 535.2565.

2-(3,4-Dimethoxyphenyl)-*N*-(naphthalene-1-yl)quinolone-4-carboxamide (5l): Off-white solid. Yield 73%. Mp 226.9-228.6 ℃. ^{1}H NMR (400 MHz,DMSO-d_6) δ 10.87 (s, 1H), 8.50 (s, 1H),8.26 (d, *J* = 8.2 Hz, 1H), 8.22-8.16 (m, 2H), 8.02-8.01 (m, 3H), 7.93 (dd, *J* = 12.5, 7.8 Hz, 2H), 7.84 (t, *J* = 7.5 Hz, 1H), 7.69-7.56 (m, 4H), 7.17 (d, *J* = 7.1 Hz, 1H),3.95 (s, 3H), 3.87 (s, 3H). ^{13}CNMR (101 MHz, DMSO) δ 166.9, 153.1, 151.2, 149.6, 148.4, 143.4, 134.3, 133.5, 131.4, 130.6, 129.9, 128.9, 128.6, 127.4, 126.8, 126.7, 126.6, 126.1, 125.6, 123.7, 123.6, 121.1, 117.2, 112.2, 111.0, 56.2, 56.1. HRMS m/z (ESI) calcd for $C_{28}H_{23}N_2O_3$ $[M+H]^+$ 435.1703 found: 435.1714, calcd for $C_{28}H_{22}N_2O_3Na$ $[M+Na]^+$ 457.1523 found: 457.1532.

2-(3,4-Dimethoxyphenyl)-*N*-(naphthalene-2-yl)quinolone-4-carboxamide (5m): Off-white solid. Yield 71%. Mp 215.9-216.4 ℃. ^{1}H NMR (400 MHz, DMSO-d_6) δ 11.04 (s, 1H), 8.60 (d, *J* = 2.1 Hz, 1H), 8.41 (s, 1H), 8.17 (t, *J* = 8.3 Hz, 2H),8.00-7.89 (m, 5H), 7.85-7.80 (m, 2H), 7.64 (t, *J* = 8.2 Hz, 1H), 7.53 (t, *J* = 7.0 Hz, 1H), 7.46 (t, *J* = 7.1 Hz, 1H), 7.15 (d, *J* = 8.8 Hz, 1H), 3.93 (s, 3H), 3.86 (s, 3H). ^{13}C NMR (101 MHz, DMSO) δ 166.2, 156.1, 151.2, 149.6, 148.3, 143.4, 137.0, 133.8, 131.3, 130.7, 130.0, 128.9, 128.0, 127.4, 127.0, 125.5, 123.4, 121.0, 120.9, 117.0, 116.8, 112.2, 110.9, 56.2, 56.1. HRMS m/z (ESI) calcd for $C_{28}H_{23}N_2O_3$ $[M+H]^+$ 435.1703 found: 435.1718, calcd for $C_{28}H_{22}N_2O_3Na$ $[M+Na]^+$ 457.1523 found: 457.1548.

Methyl (2S,3S)-3-[2-(3,4-dimethoxyphenyl)quinoline-4-amido] bicycle

[2.2.2]octane-2-carboxylate (5n): White solid. Yield 68%. Mp 185.9-187.2 ℃. ^{1}H NMR (400 MHz,DMSO-d_6) δ 8.85 (d, J = 7.0 Hz, 1H), 8.09 (d, J = 8.4 Hz, 1H), 8.06 (s, 1H), 8.03 (d, J = 7.6 Hz, 1H), 7.93 (d, J = 2.0Hz, 1H), 7.88 (dd, J = 8.4, 2.0 Hz, 1H), 7.81-7.76 (m, 1H), 7.62-7.58 (m, 1H), 7.14 (d, J = 8.5 Hz, 1H), 4.50 (t, J = 6.7 Hz, 1H), 3.91 (s, 3H), 3.85 (s, 3H), 3.68 (s, 3H),2.66 (d, J = 6.5 Hz,1H), 1.93-1.90 (m, 2H), 1.82-1.75 (m, 1H), 1.67-1.57 (m, 3H), 1.54-1.39 (m, 4H). ^{13}CNMR (101 MHz, DMSO) δ 174.7, 166.9, 155.9, 151.1, 149.5, 148.2, 143.9, 131.3, 130.5, 129.8, 127.1, 125.5, 123.6, 120.9, 116.6, 112.2, 110.8, 53.2, 53.1, 52.2, 50.2, 48.5, 29.5, 28.5, 25.7, 24.3, 21.2, 19.5. HRMS m/z (ESI) calcd for $C_{28}H_{31}N_2O_5$ $[M+H]^+$ 475.2227 found: 475.2240, calcd for $C_{28}H_{30}N_2O_5Na$ $[M+Na]^+$ 497.2047 found: 497.2059.

2-(3,4-Dimethoxyphenyl)-*N*-[(1r,3s,5R,7S)-3-hydroxyadamantan-1-yl]quinoline-4-carboxamide(5o): White solid. Yield 66%. Mp 167.3-168.5 ℃. ^{1}H NMR (400 MHz,DMSO-d_6) δ 8.34 (s, 1H), 8.08 (d, J = 8.4 Hz, 1H), 8.01 (d, J = 8.7 Hz, 1H), 7.99 (s, 1H), 7.92 (d, J = 1.5 Hz, 1H), 7.88 (dd, J = 8.3, 1.9Hz, 1H), 7.77 (t, J = 7.6 Hz, 1H), 7.60 (t, J = 6.8 Hz, 1H), 7.12 (d, J = 8.5 Hz, 1H), 4.56 (s, 1H), 3.91 (s, 3H), 3.85 (s, 3H), 2.21 (br s, 2H),2.06-1.98 (m, 6H), 1.65-1.48 (m, 6H). ^{13}CNMR (101 MHz, DMSO) δ 166.8, 156.0, 151.1, 149.5, 148.2, 144.7, 131.4, 129.8, 127.0, 125.5, 123.7, 120.9, 116.1, 112.1, 110.9, 67.8, 56.2, 56.1, 55.1, 49.4, 44.7, 40.7, 35.4, 30.6. HRMS m/z (ESI) calcd for $C_{28}H_{31}N_2O_4$ $[M+H]^+$ 459.2278 found: 459.2295, calcd for $C_{28}H_{30}N_2O_4Na$ $[M+Na]^+$ 481.2098 found: 481.2123.

2-(3-Fluoro-4-methoxyphenyl)quinolone-4-carboxylic acid (7a): White solid. Yield 67%.^{1}H NMR (400 MHz, DMSO-d_6) δ 13.98 (s, 1H), 8.61 (dd, J = 8.6, 1.3 Hz, 1H), 8.45 (s, 1H), 8.23-8.11 (m, 3H), 7.84 (ddd, J = 8.4, 6.9, 1.4 Hz, 1H), 7.69 (ddd, J = 8.3, 6.8, 1.3 Hz, 1H), 7.34 (t, J = 8.7 Hz, 1H), 3.95 (s, 3H). ^{13}C NMR (101 MHz,

DMSO) δ 168.1, 154.8, 153.5, 151.1, 148.7, 138.2, 131.4, 130.7, 130.1, 128.1, 125.8, 124.3, 123.7, 119.1, 114.4, 56.6. MS m/z (ESI): 298.08 $[M+H]^+$.

2-(4-Methoxyphenyl)quinolone-4-carboxylic acid (7b): White solid. Yield 69%. ^{1}H NMR (400 MHz, DMSO-d_6) δ 13.94 (s, 1H), 8.62 (d, J = 8.5 Hz, 1H), 8.42 (s, 1H), 8.28 (d, J = 8.4 Hz, 2H), 8.13 (d, J = 8.4 Hz, 1H), 7.83 (t, J = 7.7 Hz, 1H), 7.67 (t, J = 7.7 Hz, 1H), 7.13 (d, J = 8.5 Hz, 2H), 3.86 (s, 3H). ^{13}C NMR (101 MHz, DMSO) δ 168.2, 161.4, 155.9, 148.9, 137.9, 130.8, 130.6, 130.0, 129.2, 127.7, 125.8, 123.6, 119.1, 114.8, 55.8. MS m/z (ESI): 280.10 $[M+H]^+$.

2-(Pyridin-3-yl)quinolone-4-carboxylic acid (7c): Colorless oily. Yield 43%. ^{1}H NMR (400 MHz, DMSO-d_6) δ 9.47 (d, J = 2.3 Hz, 1H), 8.73 (dd, J = 4.8, 1.6 Hz, 1H), 8.66 (dt, J = 7.9, 1.8 Hz, 2H), 8.52 (s, 1H), 8.21 (dd, J = 8.5, 1.2 Hz, 1H), 7.89 (ddd, J = 8.4, 6.8, 1.4 Hz, 1H), 7.75 (ddd, J = 8.4, 6.8, 1.3 Hz, 1H), 7.61 (ddd, J = 8.0, 4.8, 0.9 Hz, 1H). MS m/z (ESI): 251.08 $[M+H]^+$.

2-Cyclohexylquinoline-4-carboxylic acid (7d): Colorless oily. Yield 55%. ^{1}H NMR (400 MHz, DMSO-d_6) δ 13.84 (s, 1H), 8.63 (dd, J = 8.5, 1.4 Hz, 1H), 8.03 (dd, J = 8.5, 1.2 Hz, 1H), 7.84 (s, 1H), 7.78 (ddd, J = 8.4, 6.8, 1.5 Hz, 1H), 7.64 (ddd, J = 8.4, 6.9, 1.4 Hz, 1H), 2.94 (tt, J = 11.8, 3.4 Hz, 1H), 1.99-1.90 (m, 2H), 1.84 (dt, J = 12.7, 3.4 Hz, 2H), 1.78-1.70 (m, 1H), 1.64 (qd, J = 12.5, 3.2 Hz, 2H), 1.43 (qt, J = 12.4, 3.2 Hz, 2H), 1.31 (tt, J = 12.6, 3.2 Hz, 1H).^{13}C NMR (101 MHz, DMSO) δ 168.2, 166.3, 148.5, 137.1, 130.0, 129.7, 127.4, 125.8, 123.6, 121.3, 46.6, 32.5, 26.4, 26.0. MS m/z (ESI): 256.13 $[M+H]^+$.

2-Cyclopentylquinoline-4-carboxylic acid (7e): Colorless oily. Yield 61%.^{1}H NMR (400 MHz, DMSO-d_6) δ 13.79 (s, 1H), 8.61 (dd, J = 8.5, 1.3 Hz, 1H), 8.02 (dd, J = 8.5, 1.2 Hz, 1H), 7.84 (s, 1H), 7.78 (ddd, J = 8.3, 6.8, 1.4 Hz, 1H), 7.64 (ddd, J = 8.3, 6.8, 1.3 Hz, 1H), 3.44 (p, J = 8.2 Hz, 1H), 2.17-2.03 (m, 2H), 1.95-1.77 (m, 4H), 1.70

(tt, J = 6.8, 3.7 Hz, 2H). ^{13}C NMR (101 MHz, DMSO) δ 168.2, 165.8, 148.4, 136.9, 130.1, 129.6, 127.4, 125.8, 123.6, 121.9, 48.0, 33.2, 26.0. MS m/z (ESI): 242.12 $[M+H]^+$.

2-(Thiophen-2-yl)quinolone-4-carboxylic acid (7f): The specific synthesis method was the same as that of the compound **3**, and the reaction was carried out to give a pale-yellow solid compound **7a**. Yield 70%. ^{1}H NMR (400 MHz, DMSO-d_6) δ 14.03 (s, 1H), 8.58 (dd, J = 8.7, 1.3 Hz, 1H), 8.42 (s, 1H), 8.10 (dd, J = 3.7, 1.2 Hz, 1H), 8.05 (dt, J = 8.2, 1.0 Hz, 1H), 7.82 (ddd, J = 8.4, 6.9, 1.4 Hz, 1H), 7.79 (dd, J = 5.0, 1.1 Hz, 1H), 7.66 (ddd, J = 8.4, 6.9, 1.3 Hz, 1H), 7.25 (dd, J = 5.0, 3.7 Hz, 1H). ^{13}C NMR (101 MHz, DMSO) δ 167.9, 152.1, 148.6, 144.4, 138.2, 130.9, 130.7, 129.5, 129.2, 128.2, 127.9, 126.0, 123.8, 118.5. MS m/z (ESI): 256.05 $[M+H]^+$.

2-(5-Methylthiophen-2-yl)quinolone-4-carboxylic acid (7g): Pale-yellow solid. Yield 75%. ^{1}H NMR (400 MHz, DMSO-d_6) δ 13.92 (s, 1H), 8.56 (dd, J = 8.5, 1.3 Hz, 1H), 8.34 (s, 1H), 8.00 (dd, J = 8.5, 1.2 Hz, 1H), 7.88 (d, J = 3.7 Hz, 1H), 7.80 (ddd, J = 8.4, 6.9, 1.4 Hz, 1H), 7.64 (ddd, J = 8.3, 6.9, 1.3 Hz, 1H), 6.94 (dd, J = 3.6, 1.2 Hz, 1H), 2.53 (br s, 3H). ^{13}C NMR (101 MHz, DMSO) δ 167.9, 152.2, 148.6, 144.6, 142.0, 137.9, 130.8, 129.4, 128.4, 127.7, 127.6, 125.9, 123.6, 118.2, 15.9. MS m/z (ESI): 270.06 $[M+H]^+$.

2-(Furan-2-yl)quinolone-4-carboxylic acid (7h): Pale-yellow solid. Yield 70%.^{1}H NMR (400 MHz, DMSO-d_6) δ 14.02 (s, 1H), 8.65 (dd, J = 8.6, 1.3 Hz, 1H), 8.31 (s, 1H), 8.09 (dd, J = 8.5, 1.2 Hz, 1H), 8.00-7.97 (m, 1H), 7.84 (ddd, J = 8.4, 6.8, 1.4 Hz, 1H), 7.68 (ddd, J = 8.4, 6.9, 1.3 Hz, 1H), 7.46 (dd, J = 3.4, 0.7 Hz, 1H), 6.76 (dd, J = 3.5, 1.7 Hz, 1H). ^{13}C NMR (101 MHz, DMSO) δ 167.8, 152.9, 148.8, 148.5, 145.9, 137.7, 130.9, 129.8, 128.1, 126.0, 123.8, 118.4, 113.2, 111.8. MS m/z (ESI): 240.01 $[M+H]^+$.

2-(5-Methylfuran-2-yl)quinolone-4-carboxylic acid (7i): Pale-yellow solid. Yield 66%. ^{1}H NMR (400 MHz, DMSO-d_6) δ 10.86 (s, 1H), 8.27 (d, J = 2.2 Hz, 1H), 8.20 (d, J = 8.3 Hz, 1H), 8.16 (s, 1H), 8.08 (d, J = 8.4 Hz, 1H), 7.91-7.79 (m, 2H), 7.73 (dd, J = 8.5, 2.3 Hz, 1H), 7.64 (dd, J = 8.4, 6.9 Hz, 1H), 7.36 (d, J = 3.3 Hz, 1H), 6.41 (d, J = 3.2 Hz, 1H), 2.46 (s, 3H). ^{13}C NMR (101 MHz, DMSO) δ 167.8, 155.2, 151.4, 148.9, 148.5, 137.6, 130.7, 129.6, 127.7, 126.0, 123.6, 118.3, 113.1, 109.6, 14.1. MS m/z (ESI): 254.08 $[M+H]^+$.

2-(1-Benzofuran-2-yl)quinolone-4-carboxylic acid (7j): Yellow solid. Yield 69%. ^{1}H NMR (400 MHz, DMSO-d_6) δ 14.10 (s, 1H), 8.71 (dd, J = 8.6, 1.3 Hz, 1H), 8.51 (s, 1H), 8.19 (dd, J = 8.5, 1.1 Hz, 1H), 7.94 (d, J = 0.9 Hz, 1H), 7.89 (ddd, J = 8.4, 6.8, 1.5 Hz, 1H), 7.83-7.77 (m, 2H), 7.74 (ddd, J = 8.3, 6.9, 1.3 Hz, 1H), 7.46 (ddd, J = 8.5, 7.2, 1.3 Hz, 1H), 7.35 (td, J = 7.5, 0.9 Hz, 1H). ^{13}C NMR (101 MHz, DMSO) δ 167.7, 155.5, 154.5, 148.9, 148.4, 138.1, 131.0, 130.0, 128.6, 126.6, 126.1, 124.3, 124.1, 122.7, 119.2, 112.2, 107.6. MS m/z (ESI): 290.08 $[M+H]^+$.

2-(7-Methoxy-1-benzofuran-2-yl) quinolone-4-carboxylic acid (7k): White solid. Yield 65%. ^{1}H NMR (400 MHz, DMSO-d_6) δ 8.72 (dd, J = 8.6, 1.3 Hz, 1H), 8.48 (s, 1H), 8.19 (dd, J = 8.6, 1.2 Hz, 1H), 7.90 (s, 1H), 7.89 (ddd, J = 8.4, 6.8, 1.4 Hz, 1H), 7.74 (ddd, J = 8.4, 6.9, 1.3 Hz, 1H), 7.35 (dd, J = 7.8, 1.0 Hz, 1H), 7.27 (t, J = 7.8 Hz, 1H), 7.07 (dd, J = 7.9, 1.0 Hz, 1H), 4.03 (s, 3H). ^{13}C NMR (101 MHz, DMSO) δ 167.7, 154.4, 149.0, 148.4, 145.7, 144.7, 138.0, 131.0, 130.3, 130.0, 128.7, 126.1, 124.9, 124.3, 119.1, 114.5, 108.6, 107.8, 56.3. MS m/z (ESI): 320.09 $[M+H]^+$.

2-(2H-1,3-benzodioxol-5-yl)quinolone-4-carboxylic acid (7l): White solid. Yield 72%. ^{1}H NMR (400 MHz, DMSO-d_6) δ 8.60 (dd, J = 8.5, 1.3 Hz, 1H), 8.39 (s, 1H), 8.12 (dd, J = 8.5, 1.2 Hz, 1H), 7.90-7.79 (m, 3H), 7.67 (ddd, J = 8.3, 6.8, 1.4 Hz, 1H), 7.10 (d, J = 8.1 Hz, 1H), 6.14 (s, 2H). ^{13}C NMR (101 MHz, DMSO) δ 168.2, 155.7,

149.5, 148.7, 138.3, 132.7, 130.6, 130.1, 127.9, 125.8, 123.7, 122.3, 119.2, 109.1, 107.5, 102.0. MS m/z (ESI): 294.05 $[M+H]^+$.

2-(2,3-Dihydro-1,4-benzodioxin-6-yl)quinolone-4-carboxylic acid (7m): White solid. Yield 69%. ^{1}H NMR (400 MHz, DMSO-d_6) δ 8.61 (dd, J = 8.5, 1.3 Hz, 1H), 8.37 (s, 1H), 8.12 (dd, J = 8.5, 1.2 Hz, 1H), 7.88-7.76 (m, 3H), 7.67 (ddd, J = 8.4, 6.9, 1.3 Hz, 1H), 7.04 (d, J = 8.3 Hz, 1H), 4.34 (br s, 4H). ^{13}C NMR (101 MHz, DMSO) δ 168.1, 155.6, 148.8, 145.8, 144.3, 138.1, 131.7, 130.6, 130.1, 127.8, 125.8, 123.6, 120.9, 119.1, 118.0, 116.2, 64.9, 64.6. MS m/z(ESI): 308.09 $[M+H]^+$.

***N*-[2-Chloro-5-(trifluoromethyl)phenyl]-2-(3-fluoro-4-methoxyphenyl)quinolone-4-carboxamide (8a):** White solid. Yield 48%. Mp 205.1-205.9 ℃. ^{1}H NMR (400 MHz,DMSO-d_6) δ 10.83 (s, 1H), 8.44 (s, 1H), 8.28-8.15 (m, 5H), 7.89-7.83 (m, 2H), 7.73 (dd, J = 8.3,1.3Hz, 1H), 7.68 (t, J = 8.0Hz, 1H), 7.39 (t, J = 8.6Hz, 1H),3.96(s, 3H). ^{13}CNMR (101 MHz, DMSO) δ 166.4, 154.7, 153.5, 151.1, 149.4, 148.2, 142.6, 135.9, 133.7, 131.5, 130.9, 130.0, 128.9, 128.6, 127.8, 125.6, 125.2, 124.8, 124.4, 123.5, 117.3, 115.0, 114.5, 56.7. HRMS m/z (ESI) calcd for $C_{24}H_{16}ClF_4N_2O_2$ $[M+H]^+$ 475.0831 found: 475.0845, calcd for $C_{24}H_{15}ClF_4N_2O_2Na$ $[M+Na]^+$ 497.0650 found: 497.0658.

***N*-[2-Chloro-5-(trifluoromethyl)phenyl]-2-(4-methoxyphenyl)quinoline-4-carboxamide (8b):** White solid. Yield 56%. Mp 205.7-207.1 ℃. ^{1}H NMR (400 MHz,DMSO-d_6) δ 10.83 (s, 1H), 8.39 (s, 1H), 8.33 (d, J = 8.8 Hz, 2H), 8.28 (d, J = 1.2 Hz,1H), 8.25 (d, J = 8.0Hz, 1H), 8.14 (d, J = 8.3Hz, 1H), 7.89-7.82 (m, 2H), 7.73 (dd, J = 8.4, 1.6 Hz, 1H), 7.68-7.64 (m, 1H), 7.16 (d, J = 8.9 Hz, 2H), 3.87 (s, 3H). ^{13}CNMR (101 MHz, DMSO) δ 166.5, 161.4, 155.9, 148.4, 142.4, 135.9, 133.7, 131.5, 131.0, 130.8, 129.9, 129.3, 128.9, 128.6, 127.5, 125.5, 125.3, 124.8, 123.3, 117.3,

114.8, 55.8. HRMS m/z (ESI) calcd for $C_{24}H_{17}ClF_3N_2O_2$ $[M+H]^+$ 457.0925 found: 457.0951, calcd for $C_{24}H_{16}ClF_3N_2O_2Na$ $[M+Na]^+$ 479.0745 found: 479.0740.

***N*-[2-Chloro-5-(trifluoromethyl)phenyl]-2-(pyridin-3-yl)quinolone-4-carboxamide (8c):** White solid. Yield 29%. Mp 251.3-252.4 ℃. ^{1}H NMR (400 MHz,DMSO-d_6) δ 10.87 (s, 1H), 9.53 (s, 1H), 8.75 (d, J = 3.8Hz, 1H), 8.70 (d, J = 7.9Hz, 1H), 8.54 (s, 1H), 8.31 (t, J = 6.5 Hz, 2H), 8.22 (d, J = 8.3Hz, 1H),7.92-7.87 (m, 2H), 7.74 (t, J = 7.5 Hz, 2H), 7.64 (q, J = 7.7, 4.8Hz, 1H). ^{13}CNMR (101 MHz, DMSO) δ 166.3, 154.2, 151.2, 148.9, 148.4, 142.9, 135.9, 135.1, 134.1, 133.7, 131.5, 131.1, 130.2, 128.9, 128.6, 128.4, 125.7, 125.2, 124.8, 124.5, 123.9, 117.8. HRMS m/z (ESI) calcd for $C_{22}H_{14}ClF_3N_3O$ $[M+H]^+$428.0772 found: 428.0764, calcd for $C_{22}H_{13}ClF_3N_3ONa$ $[M+Na]^+$450.0591 found: 450.0600.

***N*-[2-Chloro-5-(trifluoromethyl)phenyl]-2-cyclohexylquinoline-4-carboxamide (8d):** Colorless oily semi-solid. Yield 25%. Mp 126.6-128.3 ℃. ^{1}H NMR (400 MHz,DMSO-d_6) δ 10.74 (s, 1H), 8.23-8.21 (m, 2H), 8.04 (d, J = 8.4 Hz, 1H), 7.86 (d, J = 8.4Hz, 1H), 7.81-7.70 (m, 3H), 7.63 (t, J = 7.30 Hz, 1H), 2.95 (t, J = 11.6 Hz, 1H),1.99 (d, J = 11.9 Hz, 2H), 1.86 (d, J = 12.8 Hz, 2H), 1.77-1.65 (m, 3H), 1.49-1.40 (m, 2H), 1.34 (d, J = 12.4 Hz, 1H). ^{13}CNMR (101 MHz, DMSO) δ 166.6, 166.3, 148.0, 141.9, 135.9, 133.8, 131.4, 130.2, 129.5, 128.9, 128.6, 127.1, 125.5, 125.4, 125.3, 124.7, 123.3, 122.7, 119.1, 46.9, 32.5, 26.4, 26.1. HRMS m/z (ESI) calcd for $C_{23}H_{21}ClF_3N_2O$ $[M+H]^+$ 433.1289 found: 433.1251, calcd for $C_{23}H_{20}ClF_3N_2ONa$ $[M+Na]^+$ 455.1108 found: 455.1088.

***N*-[2-Chloro-5-(trifluoromethyl)phenyl]-2-cyclopentylquinoline-4-carboxamide (8e):** Colorless oily semi-solid. Yield 23%. Mp 187.9-189.6 ℃. ^{1}H NMR (400 MHz,DMSO-d_6) δ 10.76 (s, 1H), 8.25 (s, 1H), 8.21 (d, J = 8.4 Hz, 1H), 8.14 (s, 1H), 8.08-8.01 (m, 1H), 7.90-7.85 (m, 1H), 7.79 (ddd, J = 8.3, 6.8, 1.4 Hz, 1H), 7.75-7.70

(m, 1H), 7.64 (ddd, *J* = 8.2, 6.9, 1.3 Hz, 1H), 3.01-2.88 (m, 2H), 2.70-2.55 (m, 3H), 2.11-1.91 (m, 3H), 0.84 (q, *J* = 5.3, 4.4 Hz, 1H). HRMS m/z (ESI) calcd for $C_{22}H_{19}ClF_3N_2O$ $[M+H]^+$ 419.1133 found: 419.0959, calcd for $C_{22}H_{18}ClF_3N_2ONa$ $[M+Na]^+$ 441.0952 found: 441.0790.

***N*-[2-Chloro-5-(trifluoromethyl)phenyl]-2-(thiophen-2-yl)quinoline-4-carboxamide (8f):** White solid. Yield 51%. Mp 252.2-253.6 ℃. ^{1}H NMR (400 MHz,DMSO-d_6) δ10.85 (s, 1H), 8.39 (s, 1H),8.28 (d, *J* = 1.2 Hz, 1H), 8.21 (d, *J* = 6.9 Hz, 1H), 8.08 (dd, *J* = 11.5, 5.7Hz, 2H), 7.89-7.79 (m, 3H), 7.73 (dd, *J* = 8.5,2.2Hz, 1H), 7.68-7.64 (m, 1H), 7.28 (dd, *J* = 4.9, 3.7 Hz, 1H). ^{13}CNMR (101 MHz, DMSO) δ 166.3, 152.1, 148.1, 144.6, 142.7, 135.8, 133.5, 131.5, 131.1, 130.7, 129.4, 129.1, 128.9, 128.6, 128.2, 127.7, 125.7, 125.1, 124.7, 123.6, 116.6. HRMS m/z (ESI) calcd for $C_{21}H_{13}ClF_3N_2OS$ $[M+H]^+$ 433.0384 found: 433.0391, calcd for $C_{21}H_{12}ClF_3N_2OSNa$ $[M+Na]^+$ 455.0203 found: 455.0217.

***N*-[2-Chloro-5-(trifluoromethyl)phenyl]-2-(5-methylthiophen-2-yl)quinolone-4-carboxamide (8g):** White solid. Yield 46%. Mp 216.1-217.9 ℃. ^{1}H NMR (400 MHz,DMSO-d_6) δ 10.84 (s, 1H), 8.31 (s, 1H), 8.27 (s, 1H), 8.20 (d, *J* = 8.1Hz, 1H), 8.02 (d, *J* = 8.4Hz, 1H), 7.88 (t, *J* = 6.9Hz, 2H), 7.83-7.78 (m, 1H), 7.72 (dd, *J* = 8.4,1.5Hz, 1H), 7.63 (t, *J* = 8.1Hz, 1H),6.97 (dd, *J* = 3.6,1.0Hz, 1H), 2.54 (s, 3H). ^{13}CNMR (101 MHz, DMSO) δ 166.3, 152.2, 148.1, 144.6, 142.5, 142.2, 135.9, 131.5, 130.9, 129.3, 128.9, 128.5, 128.4, 127.6, 127.4, 125.7, 125.5, 125.0, 124.7, 123.4, 116.3, 15.9. HRMS m/z (ESI) calcd for $C_{22}H_{15}ClF_3N_2OS$ $[M+H]^+$ 447.0540 found: 447.0541, calcd for $C_{22}H_{14}ClF_3N_2OSNa$ $[M+Na]^+$ 469.0360 found: 469.0440.

***N*-[2-Chloro-5-(trifluoromethyl)phenyl]-2-(furan-2-yl)quinoline-4-carboxamide (8h):** White solid. Yield 49%. Mp 189.9-190.5 ℃. ^{1}H NMR (400 MHz,DMSO-d_6) δ 10.87 (s, 1H), 8.29-8.23 (m, 3H), 8.10 (d, *J* = 8.3Hz, 1H), 8.00 (d, *J* = 1.0Hz, 1H),

7.88-7.83 (m, 2H), 7.73 (dd, *J* = 8.9, 2.0 Hz, 1H), 7.69-7.65 (m, 1H), 7.46 (d, *J* = 3.3Hz, 1H),6.79 (dd, *J* = 5.5,1.8 Hz, 1H). ^{13}CNMR (101 MHz,DMSO) δ 166.2, 153.1, 148.5, 148.3, 145.9, 142.6, 135.8, 133.7, 131.5, 131.1, 129.6, 128.9. 128.6, 127.8, 125.7, 125.3, 124.8, 123.5, 116.2, 113.3, 111.8.HRMS m/z (ESI) calcd for $C_{21}H_{13}ClF_3N_2O_2$ $[M+H]^+$ 417.0612 found: 417.0589, calcd for $C_{21}H_{12}ClF_3N_2O_2Na$ $[M+Na]^+$ 439.0432 found: 439.0428.

***N*-[2-Chloro-5-(trifluoromethyl)phenyl]-2-(5-methylfuran-2-yl)quinoline-4-carboxamide (8i):** White solid. Yield 55%. Mp 208.9-209.9 ℃. ^{1}H NMR (400 MHz,DMSO-d_6) δ 10.85 (s, 1H), 8.27 (s, 1H), 8.21 (d, *J* = 8.2Hz, 1H), 8.16 (s, 1H), 8.08 (d, *J* = 8.4 Hz, 1H), 7.88-7.80 (m, 2H), 7.72 (d, *J* = 8.8Hz, 1H),7.64 (t, *J* = 7.4 Hz, 1H), 7.36 (d, *J* = 3.2 Hz, 1H), 6.40 (d, *J* = 2.6 Hz, 1H), 2.45 (s, 3H). ^{13}CNMR (101 MHz, DMSO) δ 166.3, 155.2, 151.6, 148.5, 148.3, 142.5, 135.8, 133.7, 131.5, 131.0, 129.5, 128.9, 128.6, 127.4, 125.7, 125.2, 124.8, 123.3, 116.1, 113.2, 109.6, 14.1. HRMS m/z (ESI) calcd for $C_{22}H_{15}ClF_3N_2O_2$ $[M+H]^+$ 431.0769 found: 431.0791, calcd for $C_{22}H_{14}ClF_3N_2O_2Na$ $[M+Na]^+$ 453.0588 found: 455.0627.

2-(1-Benzofuran-2-yl)-*N*-[2-chloro-5-(trifluoromethyl)phenyl]quinolone-4-carboxamide (8j): White solid. Yield 55%. Mp 245.1-246.9 ℃. ^{1}H NMR (400 MHz,DMSO-d_6) δ 10.94 (s, 1H), 8.46 (s, 1H), 8.32 (s, 1H), 8.29 (d, *J* = 8.4Hz, 1H), 8.21 (d, *J* = 8.40 Hz, 1H), 7.95 (s, 1H), 7.93-7.88 (m, 2H), 7.82 (dd, *J* = 7.7 Hz, 1.1 Hz, 1H), 7.78 (d, *J* = 8.3Hz, 1H),7.77-7.72 (m, 2H), 7.49-7.45 (m, 1H),7,36 (t, *J*= 9.5 Hz, 1H). ^{13}CNMR (101 MHz, DMSO) δ 166.1, 155.5, 154.9, 148.4, 142.8, 135.8, 133.7, 131.5, 131.3, 129.9, 128.9, 128.8, 128.6, 128.4, 126.7, 125.8, 125.3, 124.9, 124.8, 124.0, 122.7, 117.1, 112.2, 107.1. HRMS m/z (ESI) calcd for $C_{25}H_{15}ClF_3N_2O_2$ $[M+H]^+$ 467.0769 found: 467.0782, calcd for $C_{25}H_{14}ClF_3N_2O_2Na$ $[M+Na]^+$ 489.0583 found: 489.0616.

***N*-[2-Chloro-5-(trifluoromethyl)phenyl]-2-(7-methoxy-1-benzofuran-2-yl)quinolone-4-carboxamide (8k):** White solid. Yield 41%. Mp 254.6-255.9 ℃. ^{1}H NMR (400 MHz,DMSO-d_6) δ 10.93 (s, 1H), 8.43 (s, 1H), 8.31 (t, J = 8.8Hz, 2H), 8.21 (d, J = 8.4Hz, 1H), 7.95-7.87 (m, 3H), 7.76-7.71 (m,2H), 7.37 (d, J = 7.3Hz, 1H),7.27 (t, J = 7.9 Hz, 1H), 7.07 (d, J = 7.6 Hz, 1H), 4.02 (s, 3H). ^{13}CNMR (101 MHz, DMSO) δ 166.1, 154.7, 148.4, 148.3, 145.7, 144.8, 142,9, 135.9, 133.6, 131.5, 131.3, 130.3, 129.9, 128.6, 128.4, 125.8, 125.3, 125.0, 124.7, 124.0, 122.8, 117.0, 114.6, 108.7, 108.1, 56.3. HRMS m/z (ESI) calcd for $C_{26}H_{17}ClF_3N_2O_3$ $[M+H]^+$ 497.0874 found: 497.0833, calcd for $C_{26}H_{16}ClF_3N_2O_3Na$ $[M+Na]^+$519.0694 found: 519.0660.

2-(2*H*-1,3-Benzodioxol-5-yl)-*N*-[2-chloro-5-(trifluoromethyl)phenyl]quinolone-4-carboxamide (8l): White solid. Yield 56%. Mp 196.5-197.7 ℃. ^{1}H NMR (400 MHz,DMSO-d_6) δ 10.81 (s, 1H), 8.39 (s, 1H), 8.27-8.24 (m, 2H), 8.14 (d, J = 8.4Hz, 1H), 7.94-7.92 (m, 2H), 7.85 (dd, J = 17.9, 7.8Hz, 2H), 7.73 (dd, J = 8.3, 1.3Hz, 1H),7.66 (t, J = 8.1 Hz, 1H), 7.14 (d, J = 8.6 Hz, 1H), 6.15(s, 2H). ^{13}CNMR (101 MHz, DMSO) δ 166.5, 155.6, 149.5, 148.7, 148.3, 142.4, 135.9, 133.7, 132.9, 131.5, 130.8, 129.9, 128.9, 128.6, 127.6, 125.5, 125.3, 124.7, 123.4, 122.4, 117.5, 109.1, 107.6, 102.1. HRMS m/z (ESI) calcd for $C_{24}H_{15}ClF_3N_2O_3$ $[M+H]^+$ 471.0718 found: 471.0711, calcd for $C_{24}H_{14}ClF_3N_2O_3Na$ $[M+Na]^+$ 493.0537 found: 493.0538.

***N*-[2-Chloro-5-(trifluoromethyl)phenyl]-2-(2,3-dihydro-1,4-benzodioxin-6-yl)quinolone-4-carboxamide (8m):** White solid. Yield 55%. Mp 201.7-203.2 ℃. ^{1}H NMR (400 MHz,DMSO-d_6) δ 10.81 (s, 1H), 8.38 (s, 1H), 8.26 (t, J = 7.9Hz, 2H), 8.13 (d, J = 8.4Hz, 1H), 7.90-7.81 (m, 4H), 7.73 (dd, J = 8.5,1.7Hz, 1H), 7.66 (t, J = 7.6Hz, 1H),7.07 (d, J = 8.4 Hz, 1H), 4.34(s, 4H). ^{13}CNMR (101 MHz, DMSO) δ 166.5, 155.6, 148.3, 145.8, 144.3, 142.3, 135.9, 133.8, 131.9, 131.5, 130.7, 129.9, 128.9, 128.6, 127.6, 125.5, 124.7, 123.4, 122.8, 121.0, 118.0, 117.3, 116.4, 64.9, 64.6. HRMS m/z

(ESI) calcd for $C_{25}H_{17}ClF_3N_2O_3$ $[M+H]^+$ 485.0874 found: 485.0866, calcd for $C_{25}H_{16}ClF_3N_2O_3Na$ $[M+Na]^+$ 507.0694 found: 507.0700.

2-(1-Benzofuran-2-yl)-*N*-(3,4-dichlorophenyl)quinolone-4-carboxamide (12a): White solid. Yield 37%. Mp >290 ℃. ^{1}H NMR (400 MHz, DMSO-d_6) δ 11.19 (s, 1H), 8.40 (s, 1H), 8.28-8.14 (m, 3H), 8.01-7.95 (m, 1H), 7.90 (ddd, J = 8.4, 6.8, 1.5 Hz, 1H), 7.84-7.67 (m, 5H), 7.46 (ddd, J = 8.4, 7.2, 1.4 Hz, 1H), 7.41-7.33 (m, 1H). ^{13}C NMR (101 MHz, DMSO) δ 165.7, 155.5, 154.6, 148.4, 142.9, 139.3, 131.6, 131.4, 131.3, 130.0, 128.7, 128.5, 126.7, 126.3, 125.7, 124.2, 123.7, 122.7, 121.8, 120.6, 116.9, 112.2, 108.0. HRMS m/z (ESI) calcd for $C_{24}H_{15}Cl_2N_2O_2$ $[M+H]^+$ 433.0505 found: 433.0532, calcd for $C_{24}H_{14}Cl_2N_2O_2Na$ $[M+Na]^+$ 455.0325 found: 455.0329.

2-(1-Benzofuran-2-yl)-*N*-(2,3-dichlorophenyl)quinoline-4-carboxamide (12b): White solid. Yield 34%. Mp >290 ℃. ^{1}H NMR (400 MHz, DMSO-d_6) δ 10.87 (s, 1H), 8.39 (s, 1H), 8.27 (d, J = 8.3 Hz, 1H), 8.20 (d, J = 8.4 Hz, 1H), 7.96 (s, 1H), 7.91 (ddd, J = 8.4, 6.9, 1.4 Hz, 1H), 7.81 (dd, J = 12.8, 8.1 Hz, 3H), 7.74 (ddd, J = 8.2, 6.9, 1.3 Hz, 1H), 7.65 (dd, J = 8.1, 1.5 Hz, 1H), 7.55-7.44 (m, 2H), 7.39-7.33 (m, 1H). HRMS m/z (ESI) calcd for $C_{24}H_{15}Cl_2N_2O_2$ $[M+H]^+$ 433.0505 found: 433.0507, calcd for $C_{24}H_{14}Cl_2N_2O_2Na$ $[M+Na]^+$ 455.0325 found: 455.0329.

2-(1-Benzofuran-2-yl)-*N*-(3-chloro-2-methylphenyl)quinoline-4-carboxamide (12c): White solid. Yield 35%. Mp >290 ℃. ^{1}H NMR (400 MHz, DMSO-d_6) δ 10.65 (s, 1H), 8.41 (s, 1H), 8.22 (dd, J = 13.7, 8.4 Hz, 2H), 7.99 (s, 1H), 7.90 (ddd, J = 8.4, 6.8, 1.4 Hz, 1H), 7.81 (dd, J = 13.5, 8.0 Hz, 2H), 7.73 (ddd, J = 8.2, 6.8, 1.3 Hz, 1H), 7.59 (d, J = 7.8 Hz, 1H), 7.51-7.41 (m, 2H), 7.35 (q, J = 8.1 Hz, 2H), 2.40 (s, 3H). ^{13}C NMR (101 MHz, DMSO) δ 165.9, 155.5, 154.7, 148.4, 143.4, 137.7, 134.4, 132.1, 131.3, 130.0, 128.8, 128.4, 127.6, 126.7, 126.0, 125.7, 124.2, 124.1, 122.7, 116.8, 112.2, 107.9, 15.9. HRMS m/z (ESI) calcd for $C_{25}H_{18}ClN_2O_2$ $[M+H]^+$ 413.1051 found:

413.1055, calcd for $C_{25}H_{17}ClN_2O_2Na$ $[M+Na]^+$ 435.0871 found: 435.0874.

2-(1-Benzofuran-2-yl)-*N*-(2,5-dimethylphenyl)quinoline-4-carboxamide (12d): White solid. Yield 19%. Mp >290 ℃. ^{1}H NMR (400 MHz, DMSO-d_6) δ 10.33 (s, 1H), 8.36 (s, 1H), 8.27-8.16 (m, 2H), 7.98 (d, J = 1.0 Hz, 1H), 7.90 (ddd, J = 8.4, 6.8, 1.4 Hz, 1H), 7.81 (dd, J = 12.2, 8.0 Hz, 2H), 7.73 (ddd, J = 8.2, 6.9, 1.3 Hz, 1H), 7.47 (ddd, J = 8.3, 7.2, 1.3 Hz, 1H), 7.44-7.40 (m, 1H), 7.40-7.32 (m, 1H), 7.21 (d, J = 7.7 Hz, 1H), 7.05 (dd, J = 7.7, 1.8 Hz, 1H), 2.35 (s, 3H), 2.32 (s, 3H). ^{13}C NMR (101 MHz, DMSO) δ 165.6, 155.5, 154.7, 148.4, 143.9, 135.9, 135.7, 131.2, 130.8, 130.5, 129.9, 128.8, 128.3, 127.5, 127.2, 126.7, 125.8, 124.2, 122.7, 116.6, 112.2, 107.9, 21.0, 18.1. HRMS m/z (ESI) calcd for $C_{26}H_{21}N_2O_2$ $[M+H]^+$ 393.1598 found: 393.1600, calcd for $C_{26}H_{20}N_2O_2Na$ $[M+Na]^+$ 415.1417 found: 415.1425.

2-(1-Benzofuran-2-yl)-*N*-(2,4,6-trimethylphenyl)quinolone-4-carboxamide (12e): White solid. Yield 21%. Mp 266.8-268.1 ℃. ^{1}H NMR (400 MHz, DMSO-d_6) δ 10.21 (s, 1H), 8.30 (s, 1H), 8.25 (dd, J = 8.4, 1.3 Hz, 1H), 8.20 (d, J = 8.4 Hz, 1H), 7.99 (d, J = 0.9 Hz, 1H), 7.90 (ddd, J = 8.4, 6.9, 1.4 Hz, 1H), 7.85-7.78 (m, 2H), 7.74 (ddd, J = 8.3, 6.9, 1.2 Hz, 1H), 7.50-7.44 (m, 1H), 7.40-7.33 (m, 1H), 7.00 (s, 2H), 2.34 (s, 6H), 2.29 (s, 3H). ^{13}C NMR (101 MHz, DMSO) δ 165.5, 155.5, 154.6, 148.5, 148.4, 143.9, 136.6, 135.5, 132.2, 131.3, 130.0, 129.0, 128.8, 128.4, 126.7, 125.8, 124.2, 122.7, 116.4, 112.2, 107.9, 21.0, 18.8. HRMS m/z (ESI) calcd for $C_{27}H_{23}N_2O_2$ [M+H]+ 407.1754 found: 407.1760, calcd for $C_{27}H_{22}N_2O_2Na$ [M+Na]+ 429.1573 found: 429.1572.

2-(1-Benzofuran-2-yl)-*N*-(3-fluorophenyl)quinolone-4-carboxamide (12f): White solid. Yield 20%. Mp 295.3-296.9 ℃. ^{1}H NMR (400 MHz, DMSO-d_6) δ 11.10 (s, 1H), 8.38 (s, 1H), 8.18 (dd, J = 14.9, 8.3 Hz, 2H), 8.05-7.66 (m, 6H), 7.62-7.30 (m, 4H), 7.03 (t, J = 8.6 Hz, 1H). ^{13}C NMR (101 MHz, DMSO) δ 165.7, 155.5, 154.6,

148.4, 143.2, 131.3, 130.0, 128.7, 128.5, 126.7, 125.7, 124.2, 123.8, 122.7, 116.8, 116.3, 112.2, 108.0. HRMS m/z (ESI) calcd for $C_{24}H_{16}FN_2O_2$ $[M+H]^+$ 383.1190 found: 383.1194, calcd for $C_{24}H_{15}FN_2O_2Na$ $[M+Na]^+$ 405.1010 found: 405.1017.

2-(1-Benzofuran-2-yl)-*N*-[3,5-bis(trifluoromethyl)phenyl]quinolone-4-carboxamide (12h): White solid. Yield 26%. Mp 271.2-272.9 ℃. ^{1}H NMR (400 MHz,DMSO-d_6) δ 11.52 (s, 1H), 8.51 (d, J = 17.0 Hz, 3H), 8.25 (dt, J = 21.1, 8.0 Hz, 2H), 8.04-7.89 (m, 3H), 7.80 (dd, J = 18.1, 7.9 Hz, 2H), 7.73 (t, J = 7.7 Hz, 1H), 7.53-7.44 (m, 1H), 7.36 (t, J = 7.5 Hz, 1H). ^{13}CNMR (101 MHz, DMSO) δ 166.2, 155.5, 154.6, 148.5, 148.4, 142.4, 141.1, 131.4, 131.2, 130.0, 128.7, 128.6, 126.7, 125.8, 124.2, 122.8, 120.4, 117.1, 112.2, 108.0. HRMS m/z (ESI) calcd for $C_{26}H_{15}F_6N_2O_2$ $[M+H]^+$501.1032 found: 501.1031, calcd for $C_{26}H_{14}F_6N_2O_2Na$ $[M+Na]^+$523.0852 found: 523.0868.

2-(1-Benzofuran-2-yl)-*N*-[2-chloro-4-(trifluoromethyl)phenyl]quinolone-4-carboxamide (12i): White solid. Yield 44%. Mp 249.1-249.9 ℃. ^{1}H NMR (400 MHz, DMSO-d_6) δ 10.96 (s, 1H), 8.44 (s, 1H), 8.22 (tdd, J = 21.0, 12.5, 6.0 Hz, 3H), 8.06 (d, J = 2.2 Hz, 1H), 7.98-7.69 (m, 6H), 7.49 (dt, J = 15.0, 7.6 Hz, 1H), 7.36 (t, J = 7.4 Hz, 1H). HRMS m/z (ESI) calcd for $C_{25}H_{15}ClF_3N_2O_2$ $[M+H]^+$ 467.0769 found: 467.0774, calcd for $C_{25}H_{14}ClF_3N_2O_2Na$ $[M+Na]^+$ 489.0588 found: 489.0929.

2-(1-Benzofuran-2-yl)-*N*-(4-ethoxyphenyl)quinoline-4-carboxamide (12j): White solid. Yield 36%. Mp >290 ℃. ^{1}H NMR (400 MHz, DMSO-d_6) δ 10.74 (s, 1H), 8.34 (s, 1H), 8.18 (t, J = 7.6 Hz, 2H), 7.98 (s, 1H), 7.93-7.85 (m, 1H), 7.79 (dd, J = 12.2, 8.1 Hz, 2H), 7.74-7.68 (m, 3H), 7.46 (t, J = 7.9 Hz, 1H), 7.35 (t, J = 7.5 Hz, 1H), 6.98 (d, J = 8.9 Hz, 2H), 4.04 (q, J = 6.9 Hz, 2H), 1.35 (t, J = 7.0 Hz, 3H). HRMS m/z (ESI) calcd for $C_{26}H_{21}N_2O_3$ $[M+H]^+$ 409.1547 found: 409.1547, calcd for $C_{26}H_{20}N_2O_3Na$ $[M+Na]^+$ 431.1366 found: 431.1220.

2-(1-Benzofuran-2-yl)-*N*-[(3,4-dichlorophenyl)methyl]quinoline-4-carboxamide (12k): White solid. Yield 49%. Mp 229.8-231.2 ℃. ^{1}H NMR (400 MHz, DMSO-d_6) δ 9.52 (t, J = 6.0 Hz, 1H), 8.23 (s, 1H), 8.20-8.12 (m, 2H), 7.94 (s, 1H), 7.87 (ddd, J = 8.3, 6.8, 1.4 Hz, 1H), 7.79 (dd, J = 13.6, 8.0 Hz, 2H), 7.74-7.64 (m, 3H), 7.51- 7.41 (m, 2H), 7.35 (t, J = 7.5 Hz, 1H), 4.61 (d, J = 6.0 Hz, 2H). ^{13}C NMR (101 MHz, DMSO) δ 167.0, 155.5, 154.7, 148.4, 143.2, 140.7, 131.5, 131.2, 130.1, 129.9, 128.7, 128.4, 128.2, 126.6, 125.8, 124.1, 122.7, 116.6, 112.2, 107.8, 42.3. HRMS m/z (ESI) calcd for $C_{25}H_{17}Cl_2N_2O_2$ $[M+H]^+$ 447.0662 found: 447.0724, calcd for $C_{25}H_{16}Cl_2N_2O_2Na$ $[M+Na]^+$ 469.0481 found: 469.0484.

2-(1-Benzofuran-2-yl)-*N*-[(4-methylphenyl)methyl]quinoline-4-carboxamide (12l): White solid. Yield 55%. Mp 235.8-236.9 ℃. ^{1}H NMR (400 MHz, DMSO-d_6) δ 9.41 (t, J = 6.0 Hz, 1H), 8.18 (s, 1H), 8.16 (dt, J = 8.2, 1.6 Hz, 2H), 7.92 (d, J = 0.9 Hz, 1H), 7.86 (ddd, J = 8.5, 6.8, 1.4 Hz, 1H), 7.83-7.74 (m, 2H), 7.68 (ddd, J = 8.2, 6.9, 1.3 Hz, 1H), 7.45 (ddd, J = 8.4, 7.2, 1.4 Hz, 1H), 7.37-7.32 (m, 3H), 7.22 (s, 1H), 7.20 (s, 1H), 4.57 (d, J = 5.9 Hz, 2H), 2.32 (s, 3H). ^{13}C NMR (101 MHz, DMSO) δ 166.8, 155.5, 154.7, 148.4, 148.3, 143.6, 136.6, 136.4, 131.1, 129.8, 129.5, 128.8, 128.1, 128.0, 126.6, 125.9, 124.2, 124.1, 122.7, 116.4, 112.2, 107.7, 43.0, 21.2. HRMS m/z (ESI) calcd for $C_{26}H_{21}N_2O_2$ $[M+H]^+$ 393.1598 found: 393.1601, calcd for $C_{26}H_{20}N_2O_2Na$ $[M+Na]^+$ 415.1417 found: 415.1427.

2-(1-Benzofuran-2-yl)-*N*-[(4-fluorophenyl)methyl]quinoline-4-carboxamide (12m): White solid. Yield 53%. Mp 225.6-226.7 ℃. ^{1}H NMR (400 MHz, DMSO-d_6) δ 9.50 (t, J = 5.9 Hz, 1H), 8.21 (s, 1H), 8.16 (dd, J = 8.3, 1.3 Hz, 2H), 7.93 (d, J = 1.0 Hz, 1H), 7.86 (ddd, J = 8.2, 6.8, 1.4 Hz, 1H), 7.83-7.74 (m, 2H), 7.68 (ddd, J = 8.2, 6.9, 1.2 Hz, 1H), 7.53-7.42 (m, 3H), 7.35 (td, J = 7.5, 1.0 Hz, 1H), 7.23 (t, J = 8.9 Hz, 2H), 4.60 (d, J = 5.8 Hz, 2H). ^{13}C NMR (101 MHz, DMSO) δ 166.8, 163.0, 160.6,

155.5, 154.7, 148.4, 148.3, 143.4, 135.7, 131.1, 130.0, 129.9, 128.7, 128.1, 126.6, 125.9, 124.2, 122.7, 116.5, 115.8, 115.6, 112.2, 107.8, 42.6. HRMS m/z (ESI) calcd for $C_{25}H_{18}FN_2O_2$ $[M+H]^+$ 397.1347 found: 397.1349, calcd for $C_{25}H_{17}FN_2O_2Na$ $[M+Na]^+$ 419.1166 found: 419.1168.

2-(1-Benzofuran-2-yl)-*N*-(naphthalene-1-yl)quinolone-4-carboxamide (12n): White solid. Yield 38%. Mp 286.9-288.3 ℃. ^{1}H NMR (400 MHz,DMSO-d_6) δ 10.98 (s, 1H), 8.52 (s, 1H), 8.30 (d,J = 8.4Hz, 1H), 8.21 (s, 2H), 8.03 (t,J = 4.3Hz, 2H), 7.92 (br s, 3H), 7.82 (t,J = 9.6Hz, 2H),7.74 (t, J = 7.1Hz, 1H), 7.65-7.57 (m, 3H), 7.47 (t, J = 7.3Hz, 1H), 7.36 (t, J = 7.0Hz, 1H). HRMS m/z (ESI) calcd for $C_{28}H_{19}N_2O_2$ $[M+H]^+$415.1441 found: 415.1451, calcd for $C_{28}H_{18}N_2O_2Na$ $[M+Na]^+$437.1260 found: 437.1272.

2-(1-Benzofuran-2-yl)-*N*-[phenyl(pyridine-2-yl)methyl]quinolone-4-carboxamide (12o): White solid. Yield 33%. Mp 222.5-223.4 ℃. ^{1}H NMR (400 MHz,DMSO-d_6) δ 9.87 (d, J = 8.2 Hz, 1H), 8.66-8.55 (m, 1H), 8.19 (s, 1H), 8.18-8.13 (m, 1H), 8.06 (d, J = 8.1 Hz, 1H), 7.94 (s, 1H), 7.85 (t, J = 7.7 Hz, 2H), 7.79 (t, J = 8.3 Hz, 2H), 7.64 (t, J = 7.6 Hz, 1H), 7.58 (d, J = 7.9 Hz, 1H), 7.50 (d, J = 7.4 Hz, 2H), 7.45 (t, J = 7.2 Hz, 1H), 7.41-7.27 (m, 5H), 6.55 (d, J = 8.2 Hz, 1H). ^{13}CNMR (101 MHz, DMSO) δ 166.5, 160.8, 155.5, 154.7, 149.6, 148.3, 143.7, 141.5, 137.6, 131.1, 129.8, 129.0, 128.8, 128.2, 128.1, 127.8, 126.6, 125.8, 124.3, 124.1, 123.0, 122.7, 122.2, 116.5, 112.2, 107.7, 59.1. HRMS m/z (ESI) calcd for $C_{30}H_{22}N_3O_2$ $[M+H]^+$ 456.1707 found: 456.1714, calcd for $C_{30}H_{21}N_3O_2Na$ $[M+Na]^+$ 478.1526 found: 478.1530.

2-(1-Benzofuran-2-yl)-*N*-(4-phenoxyphenyl)quinolone-4-carboxamide (12p): White solid. Yield 38%. Mp 264.5-265.8 ℃. ^{1}H NMR (400 MHz,DMSO-d_6) δ 10.97 (s, 1H), 8.37 (s, 1H), 8.20 (dd,J = 8.2, 3.5Hz, 2H), 7.98 (s, 1H), 7.91-7.86 (m, 3H), 7.80 (dd, J = 12.8, 8.0Hz, 2H), 7.73-7.69 (m, 1H),7.48-7.33 (m, 4H), 7.16-7.10 (m,

3H), 7.03 (d, J = 7.8Hz, 2H). ^{13}CNMR (101 MHz, DMSO) δ 165.2, 157.7, 155.5, 154.7, 153.0, 148.4, 143.6, 135.1, 131.2, 130.5, 129.9, 128.8, 128.4, 126.7, 125.8, 124.2, 124.0, 123.6, 122.7, 122.3, 120.0, 118.5, 116.8, 112.2, 107.9. HRMS m/z (ESI) calcd for $C_{30}H_{21}N_2O_3$ $[M+H]^+$ 457.1547 found: 457.1548, calcd for $C_{30}H_{20}N_2O_3Na$ $[M+Na]^+$ 479.1366 found: 479.1370.

2-(1-Benzofuran-2-yl)-*N*-(diphenylmethyl)quinolone-4-carboxamide (12q): The specific synthesis method is the same as that of the compound **5h**, and the reaction mixture gives the compound **12q** as a white solid. Yield 54%, HPLC purity 96%. Mp 248.5-249.3 ℃. ^{1}H NMR (400 MHz,DMSO-d_6) δ 9.92 (d, J = 8.6Hz, 1H), 8.18 (s, 1H), 8.16 (d,J = 8.5Hz, 1H), 7.98 (d, J = 8.3Hz, 1H), 7.95 (s, 1H), 7.87-7.83 (m, 1H), 7.79 (t,J = 9.1Hz, 2H),7.65-7.61 (m, 1H), 7.49-7.28 (m, 12H), 6.54 (d, J = 8.6Hz, 1H). ^{13}CNMR (101 MHz, DMSO) δ 166.3, 155.5, 154.7, 148.3, 143.7, 142.5, 131.1, 129.9, 129.0, 128.8, 128.1, 127.9, 127.7, 126.6, 125.6, 124.2, 124.1, 122.7, 116.4, 112.2, 107.8, 57.2. HRMS m/z (ESI) calcd for $C_{31}H_{23}N_2O_3$ $[M+H]^+$ 455.1573 found: 455.1768, calcd for $C_{31}H_{22}N_2O_2Na$ $[M+Na]^+$ 477.1573 found: 477.1593.

4.3 Pharmacological Experimental Methods

4.3.1 Protein Production and Purification

N-terminally his-tagged human SIRT6 constructs (residues 1-355, 1-318 and 13-308) using vector pQE80L.1 (internal pQE80 derivative with TEV cleavage site) or vector pET151-D-TOPO in *E. coli* M15 [pREP4] were used, which were kindly provided by Professor Clemens Steegborn (Program in Lehrstuhl Biochemie und Forschungszentrum für Biomakromoleküle Universitätsstr, Universität Bayreuth). Proteins were expressed and purified essentially as described previously.[31] The purified SIRT6 protein was stored at -80 ℃ in buffer containing 20 mM Na-HEPES pH 7.5, 100 mM NaCl, and 2 mM DTT.

4.3.2 *In vitro* Sirtuin Assay

Compounds were tested for their agonist activity against SIRT6 as described previously.[39, 43] For SIRT6 deacetylation, the 0.09 μg/mL in-house recombinant SIRT6 was incubated with different test compounds in the assay buffer (50 mM Tris–HCl, pH 8.0, 137 mM NaCl, 2.7 mM KCl, and 1 mM $MgCl_2$) in black half-volume 96-well plates at 37 ℃ for 15 min. The mixture contained 320 μM substrate S5 (Ac-RYQK(Ac)-AMC), which was purchased from CASLO ApS (Denmark). NAD (1 mM) was added to initiate the reaction, and the mixture was incubated at 37 ℃ for 120 min. Next, the developer solution containing 6 μg/μL trypsin and 40 mM nicotinamide was added, and the solutions were incubated for 30 min at room temperature. The fluorescence was then measured with excitation and emission wavelengths of 380 and 440 nm, respectively, using a Bio-Tek system (Bio-Tek Instruments, Inc., Winooski, VT). For SIRT6 fatty-acid deacetylation, 1 μM recombinant SIRT6 protein was incubated with different test compounds in the assay buffer (50 mM Tris–HCl, pH 8.0), BSA(1 mg/mL), and dithiothreitol (DTT, 1 mM)) in black, half-volume 96-well plates at 37 ℃ for 20 min. The mixture contained 10 μM Ac-EALPKK(Myr)-AMC peptide, which was purchased from ChinaPeptides Co., Ltd. (Suzhou, China). NAD (1 mM) was added to initiate the reaction, and the plates were incubated at 37 ℃ for 120 min. Next, the developer solution containing 5 mg/mL trypsin and 8 mM nicotinamide was added, and the mixtures were incubated for 120 min at 37 ℃. The fluorescence was then measured with excitation and emission wavelengths of 380 and 440 nm, respectively, using a Bio-Tek system (Bio-Tek Instruments, Inc., Winooski, VT). The experimental data were fitted in GraphPad Prism 5 to obtain inhibition or activity values using the following equations: inhibition % = (max - signal) / (max – min) * 100 or activity % = signal / (max – min)

* 100.

For SIRT6 deacetylation on Ac-RYQK(Ac)-AMC, the SIRT6 protein (60 μM) was incubated in a 100 μL reaction mixture (100 μM Ac-RYQK(Ac)-AMC, 3 mM NAD^+, and assay buffer) with DMSO or 25 μM **12q** at 37 ℃ for 5h. For SIRT6 demyristoylation on Ac-EALPKK(Myr)-AMC, the SIRT6 protein (10 μM) was incubated in a 100 μL reaction mixture (100 μM Ac-EALPKK(Myr)-AMC, 3 mM NAD^+, and assay buffer) with DMSO or 25 μM **12q** at 37 ℃ for 2 h. The reactions were quenched with 100 mM HCl and 160 mM acetic acid at 37 ℃ for 30 min. After centrifugation at 12,000 r.p.m. for 10 min, the supernatant was collected and analyzed by HPLC. HPLC analyses were performed on a ZORBAX Eclipse Plus C18 column (4.6× 100 mm, 3.5 μm). The binary solvent system (A/B) was as follows: water with 0.1% trifluoroacetic acid (A) and acetonitrile with 0.1% trifluoroacetic acid (B).

In vitro enzymatic inhibition/activation assays of SIRT1-3 were also performed using FDL assay provided by Shanghai Chempartner Co., Ltd (Shanghai, China) and in vitro enzymatic inhibition/activation assay of SIRT5 was also performed using FDL assay provided by BPS Bioscience Inc. (San Diego, California).

4.3.3 Surface Plasmon Resonance (SPR) Assay

SPR technology-based binding assays were performed on a Biacore X100 instrument (GE Healthcare) at room temperature.[51] The SIRT6 proteins were immobilized on a CM5 sensor chip by a standard amide coupling procedure in 10 mM sodium acetate (pH 4.5). The activated surface was then brought into contact with the protein solution at a concentration of 100 μg / mL. The chip was equilibrated with 1.05x PBS buffer (10.5 mM phosphate (pH 7.4), 2.84 mM KCl, 143.85 mM NaCl, and 0.005% (v/v) surfactant P20) for 4 h. The compounds were serially diluted and injected for 60 s (contact phase) at a flow rate of 30 μL/min, followed by 120 s of

buffer flow (dissociation phase). The K_D values of the tested compounds were determined by BIA evaluation software (GE Healthcare).

4.3.4 Differential Scanning Fluorimetry (DSF) Assay

DSF experiments were performed on a RT-PCR detection system (BIO-RAD CFX96) according to the known protocol.[44] SYPRO orange (Sigma, 5000X concentrate in DMSO, S5692) was monitored using FRET filters at a wavelength of 492 nm for excitation and ROX filters at a wavelength of 610 nm for emission. Each reaction solution containing 2 μM SIRT6 proteins in buffer (20 mM HEPES, pH 7.4, and 100 mM NaCl), 5 × SYPRO orange and the test compounds in 10 μL, was heated from 25 to 95 ℃. The fluorescence intensities were recorded every 1 ℃/min and plotted as a function of temperature. The inflection point of the transition curve (T_m) was calculated by fitting the Boltzmann equation to the sigmoidal curve in GraphPad Prism 5.0.

4.3.5 Isothermal Titration Calorimetry (ITC) Assay

Experiments using isothermal titration calorimetry were carried out in a MicroCal iTC200 instrument at 25 ℃.[52, 53] The buffer conditions were 20 mM HEPES (pH 7.5), 100 mM NaCl, and 2 mM DTT. The titration was performed by injecting the proteins (400 μM) into a reaction cell containing the activators (80 μM). The thermodynamic binding parameters were extracted by nonlinear regression analysis of the binding isotherms (MicroCal Origin software, version 7.0). A single-site binding model was applied to determine the equilibrium dissociation constants (K_d values).

4.3.6 Cell Culture

All the tumor cell lines used in this investigation were purchased from American Type Culture Collection (ATCC, Rockville, MD, USA). Cells were cultured in DMEM or RPMI1640 supplemented with 10% FBS (Gibco, Eggenstein, Germany),

100 units/mL penicillin (HyClone) and streptomycin (HyClone), and grown in the 37 ℃ incubator with a humidified 5% CO_2 atmosphere.[54]

4.3.7 Proliferation Assay

Cell proliferation assays were conducted as previously reported.[55] A variety of human cancer cells were plated in triplicate in 96-well plates and were treated with indicated concentrations of **12q** or other agents for 72 h, and cell viability was determined using an MTT (3-(4,5-dimethylthiazol-2-yl)-2,5-diphenyltetrazolium bromide) (Sigma-Aldrich, St. Louis, MO) assay. The IC_{50} values were calculated using GraphPad Prism 5.01 software.

4.3.8 Colony Formation Assay

The cells were seeded in 6-well plates at a density of 750, 500, 2200, and 500 cells per well for BXPC-3, PANC-1, AsPC-1, and MIAPaCa-2. After 24 h, different concentrations of **12q** or other agents were added. After 9 to 18 days of incubation, cells were fixed with 4% paraformaldehyde and stained with crystal violet. Colonies with >50 cells were counted under an inverted microscope.

4.3.9 The EdU Incorporation Assay

This EdU incorporation assay, was conducted using an EdU assay kit (KGA337-500, KeyGEN BioTECH). A total of 8000 (BXPC-3), 4600 (PANC-1), 7500 (AsPC-1), and 2500 (MIAPaCa-2) cells per well were seeded in 96-well plates and treated with different concentrations of **12q** or other agents for 24 h. Then, the proliferation of the cells was determined with an EdU-Apollo DNA proliferation detection kit according to the manufacturer's instructions. The images were captured with a high-content screening instrument (Thermo) analyzed in HCC software.

4.3.10 Migration Assay

The migration assay was performed following the method reported previously.[55,

[56] BXPC-3, PANC-1, AsPC-1, or MIAPaCa-2 cells were seeded in 12-well plates and incubated at 37 °C under 5% CO_2, and the cells were allowed to grow to monolayer confluence. Leaving the medium behind, the centers of the cell monolayer were scraped with a sterile, 200 μL pipette tip to create a denuded zone (gap) of constant width. Subsequently, the cell monolayer was washed with sterile PBS, and cells were exposed to various concentrations of **12q** or other agents. Images were taken using an Olympus inverted microscope after 24 h of incubation at 37 °C under 5% CO_2. The migrated cells were quantified by manual counting, and the percentage of inhibition was expressed using untreated wells as 100%.

4.3.11 Cellular Thermal Shift Assay (CETSA)

After treating PANC-1 cells or BXPC-3 cells with **12q** or DMSO for 72h, the cells were collected and washed twice with PBS. Resuspend the cells in PBS solution containing 1 mmol/L Cocktail. Divide each group of samples into multiple portions, corresponding to multiple temperature gradients. All samples were heated at the corresponding temperature for 3 min and then taken out. The cells were lysed by repeated freezing and thawing 3 times. The sample was then centrifuged at 12000 rpm and 4 ℃ for 15 min. The supernatants were analyzed by western blot. All experiments were performed in triplicate.

4.3.12 Western Blot Analyses

BXPC-3 and PANC-1 were incubated for 72 h in medium containing different concentrations of **12q** or other agents as previously described.[27, 33] Whole cell lysates were extracted with RIPA buffer (Beyotime, China) supplemented with protease inhibitor cocktail (Sigma-Aldrich, Merck) and PMSF (Sigma-Aldrich, Merck). Protein concentrations were determined using a BCA protein assay kit (Heart, Xi'an). The protein extracts were separated by SDS-PAGE on 12% polyacrylamide

Tris-glycine gels and transferred onto a PVDF membrane (Millipore). The PVDF membranes were then blocked with TBS-T containing 5% nonfat dry milk or 5% BSA with gentle shaking for 2 h at room temperature. Then, the membranes were incubated with antibodies including anti-SIRT6, anti-Histone H3 (acetyl K9), anti-Histone H3 (acetyl K18), anti-Histone H3 (acetyl K56), anti-Histone H3, anti-Lin28b, anti-Myc, anti-IGF2BP3, and anti-β-actin for 10 h at 4 ℃. After three washes with TBS-T, the blots were incubated with the corresponding horseradish peroxidase-linked secondary antibodies (Zhong Shan Golden Bridge Biotechnology, China) for 1 h at 37 °C with gentle shaking. After three thorough washes with TBS-T, the blots were visualized with an enhanced luminol-based chemiluminescent substrate (Abbkine). Information regarding the primary antibodies can be found in Table S4.

4.3.13 Cell Cycle Assays

Cell cycle assays in PANC-1 and BXPC-3 cells were preformed with a Cell Cycle Detection Kit (Keygentec, KGA511-KGA512) according to the manufacturer's instructions. Briefly, PANC-1 and BXPC-3 cells were seeded in 6-well plates and treated with different concentrations of **12q** or **MDL-800** for 48 h. Then, the cells were incubated with 50 μg/mL propidium iodide (PI) for 30 min in the dark. The stained cells were then analyzed using a CytoFLEX flow cytometer (Beckman Coulter) and the resulting data were analyzed with cell cycle analysis software (Kaluza, Beckman Coulter).

4.3.14 Apoptosis Assay

The apoptosis assays in PANC-1 and BXPC-3 cells were preformed with an Annexin V-FITC Apoptosis Detection Kit (Keygentec, KGA105-KGA108) according to the manufacturer's instructions. PANC-1 and BXPC-3 cells were seeded in 6-well plates and treated with different concentrations of **12q** or **MDL-800** for 48 h. Then,

the cells were incubated with 5 μL of Annexin V-FITC and 5 μL of propidium iodide for 10 min in the dark. The stained cells were then analyzed and the resulting data were analyzed using a CytoFLEX flow cytometer (Beckman Coulter).

4.3.15 Pharmacokinetic Study

A 10 or 2 mg/mL dosing solution of **12q** was prepared by dissolution in physiological saline containing 5% DMSO, 10% Solutol, and 85% saline with the pH adjusted to 7 for PO or IV administration in 6- to 8-week-old male Sprague-Dawley rats. At time points of 0.083 h, 0.25 h, 0.5 h, 1 h, 2 h, 4 h, 6 h, 8 h, and 24 h after dosing for PO or of 0.25 h, 0.5 h, 1 h, 2 h, 4 h, 6 h, 8 h, 10 h, and 24 h after dosing for IV, blood samples was collected from each animal via cardiac puncture, and plasma concentrations were determined using LC-MS/MS analysis. Noncompartmental pharmacokinetic parameters were fitted using DAS software (Enterprise, version 2.0, Mathematical Pharmacology Professional Committee of China).

4.3.16 *In Vivo* Models

All animal experiments carried out were approved by the Animal Care and Use Committee of Sichuan University (Chengdu, Sichuan, China). 6- to 8-week-old BALB/c female nude mice were purchased from Beijing HFK bioscience CO., LTD (Beijing, China). To establish the PANC-1 xenograft model, 100 μL of a PANC-1 cell suspension (between 5 x 10^6 and 1x 10^7 cells) was subcutaneously injected into the right flank region of female nude mice. After the tumors had grown to 130-150 mm^3, the mice were randomly divided into 4 groups and administered different doses of the test compound or vehicle. The compounds were dissolved in 5% (v/v) DMSO (Sigma-Aldrich), 12.5% (v/v) castor oil (Sigma-Aldrich), 12.5% ethanol, and 70% saline. Tumor burden was monitored every 3 days using calipers. Tumor volume (TV) was calculated using the following formula: TV =length $\times$ width^2 $\times$ 0.5.

ASSOCIATED CONTENT

Supporting Information

The Supporting Information is available free of charge on the ACS Publications website at http://pubs.acs.org.

Activity data of 40 candidate compounds; predicted binding mode of **Hit20** with SIRT6; dose-dependent activities of SIRT6 demyristoylation of **12q**; predicted binding mode of **12q** with SIRT6; the other experimental data of compound **12q** *in vitro* and *in vivo*; ^{1}H NMR spectra, ^{13}C NMR spectra, HRMS data and HPLC traces for key target compounds

SMILES molecular formula strings (CSV)

Binding model of compound **12q** with SIRT6 (PDB)

AUTHOR INFORMATION

Corresponding Author

*Tel.: +86-28-85164063; Fax: +86-28-85164060; E-mail: yangsy@scu.edu.cn (S.Y.).

ORCID

Shengyong Yang: 0000-0001-5147-3746

Author Contributions

‡ X.C., W. S., and S.H. contributed equally to this work.

Notes

The authors declare no competing financial interest.

ACKNOWLEDGMENTS

This work was supported by the National Natural Science Foundation of China (81773633, 21772130, and 81930125), National Science and Technology Major Project (2018ZX09711002-014-002, 2018ZX09711002-011-019, 2018ZX09201018, 2018ZX09711003-003-006, and 2019ZX09301-135), and 1.3.5 project for disciplines

of excellence, West China Hospital, Sichuan University. The authors thank Professor Clemens Steegborn (Program in Lehrstuhl Biochemie und Forschungszentrum für Biomakromoleküle Universitätsstr, Universität Bayreuth) for providing the N-Terminally his-tagged human SIRT6 constructs. The authors also thank Professor Jian Zhang (Shanghai Jiao-Tong University School of Medicine) for providing the myristoylated H3K9 (H3K9-Myr) peptide.

ABBREVIATIONS

SAR, Structure–activity relationship; HCC, Hepatocellular carcinoma cell; PKM2, Pyruvate kinase M2; PDAC, Pancreatic ductal adenocarcinoma cell; DS 3.1, Discovery Studio (DS) 3.1; $EC_{1.5}$, Concentration of compound required to increase enzyme activity by 50%; DSF, Differential Scanning Fluorimetry; SPR, Surface Plasmon Resonance; ITC, Isothermal Titration Calorimetry; MTT, (3-(4,5-dimethylthiazol-2-yl)-2,5-diphenyltetrazolium bromide); EdU, 5-ethynyl-2′-deoxyuridine.

REFERENCES

1. Schlicker, C.; Boanca, G.; Lakshminarasimhan, M.; Steegborn, C. Structure-based development of novel sirtuin inhibitors. *Aging (Albany NY)* **2011,** 3, 852-872.

2. Imai, S.-I.; Armstrong, C. M.; Kaeberlein, M.; Guarente, L. Transcriptional silencing and longevity protein Sir2 is an NAD-dependent histone deacetylase. *Nature* **2000,** 403, 795.

3. Morris, B. J. Seven sirtuins for seven deadly diseases ofaging. *Free Radical Biol. Med.* **2013,** 56, 133-171.

4. Sauve, A. A.; Wolberger, C.; Schramm, V. L.; Boeke, J. D. The biochemistry of sirtuins. *Annu. Rev. Biochem* **2006,** 75, 435-465.

5. Chalkiadaki, A.; Guarente, L. The multifaceted functions of sirtuins in cancer. *Nat. Rev. Cancer* **2015,** 15, 608-624.

6. Ferrer, C. M.; Alders, M.; Postma, A. V.; Park, S.; Klein, M. A.; Cetinbas, M.; Pajkrt, E.; Glas, A.; van Koningsbruggen, S.; Christoffels, V. M. An inactivating mutation in the histone deacetylase SIRT6 causes human perinatal lethality. *Genes Dev.* **2018,** 32, 373-388.

7. Xu, Z.; Zhang, L.; Zhang, W.; Meng, D.; Zhang, H.; Jiang, Y.; Xu, X.; Van Meter, M.; Seluanov, A.; Gorbunova, V. SIRT6 rescues the age related decline in base excision repair in a PARP1-dependent manner. *Cell cycle* **2015,** 14, 269-276.

8. Zhang, W.; Wan, H.; Feng, G.; Qu, J.; Wang, J.; Jing, Y.; Ren, R.; Liu, Z.; Zhang, L.; Chen, Z. SIRT6 deficiency results in developmental retardation in cynomolgus monkeys. *Nature* **2018,** 560, 661-665.

9. Mao, Z.; Hine, C.; Tian, X.; Van Meter, M.; Au, M.; Vaidya, A.; Seluanov, A.; Gorbunova, V. SIRT6 promotes DNA repair under stress by activating PARP1. *Science* **2011,** 332, 1443-1446.

10. Kaidi, A.; Weinert, B. T.; Choudhary, C.; Jackson, S. P. Human SIRT6 promotes DNA end resection through CtIP deacetylation. *Science* **2010,** 329, 1348-1353.

11. Mostoslavsky, R.; Chua, K. F.; Lombard, D. B.; Pang, W. W.; Fischer, M. R.; Gellon, L.; Liu, P.; Mostoslavsky, G.; Franco, S.; Murphy, M. M. Genomic instability and aging-like phenotype in the absence of mammalian SIRT6. *Cell* **2006,** 124, 315-329.

12. Michishita, E.; McCord, R. A.; Berber, E.; Kioi, M.; Padilla-Nash, H.; Damian, M.; Cheung, P.; Kusumoto, R.; Kawahara, T. L.; Barrett, J. C. SIRT6 is a histone H3 lysine 9 deacetylase that modulates telomeric chromatin. *Nature* **2008,** 452, 492-496.

13. Sebastián, C.; Zwaans, B. M.; Silberman, D. M.; Gymrek, M.; Goren, A.; Zhong,

L.; Ram, O.; Truelove, J.; Guimaraes, A. R.; Toiber, D. The histone deacetylase SIRT6 is a tumor suppressor that controls cancer metabolism. *Cell* **2012,** 151, 1185-1199.

14. Feldman, J. L.; Baeza, J.; Denu, J. M. Activation of the protein deacetylase SIRT6 by long-chain fatty acids and widespread deacylation by mammalian sirtuins. *J. Biol. Chem.* **2013,** 288, 31350-31356.

15. Kawahara, T. L.; Michishita, E.; Adler, A. S.; Damian, M.; Berber, E.; Lin, M.; McCord, R. A.; Ongaigui, K. C.; Boxer, L. D.; Chang, H. Y. SIRT6 links histone H3 lysine 9 deacetylation to NF-κB-dependent gene expression and organismal life span. *Cell* **2009,** 136, 62-74.

16. Kanfi, Y.; Naiman, S.; Amir, G.; Peshti, V.; Zinman, G.; Nahum, L.; Bar-Joseph, Z.; Cohen, H. Y. The sirtuin SIRT6 regulates lifespan in male mice. *Nature* **2012,** 483, 218-221.

17. Tian, X.; Firsanov, D.; Zhang, Z.; Cheng, Y.; Luo, L.; Tombline, G.; Tan, R.; Simon, M.; Henderson, S.; Steffan, J. SIRT6 is responsible for more efficient DNA double-strand break repair in long-lived species. *Cell* **2019,** 177, 622-638. e22.

18. Jung, E. S.; Choi, H.; Song, H.; Hwang, Y. J.; Kim, A.; Ryu, H.; Mook-Jung, I. p53-dependent SIRT6 expression protects Aβ42-induced DNA damage. *Sci. Rep.* **2016,** 6, 25628.

19. Kaluski, S.; Portillo, M.; Besnard, A.; Stein, D.; Einav, M.; Zhong, L.; Ueberham, U.; Arendt, T.; Mostoslavsky, R.; Sahay, A. Neuroprotective functions for the histone deacetylase SIRT6. *Cell Rep.* **2017,** 18, 3052-3062.

20. Zhong, L.; D'Urso, A.; Toiber, D.; Sebastian, C.; Henry, R. E.; Vadysirisack, D. D.; Guimaraes, A.; Marinelli, B.; Wikstrom, J. D.; Nir, T. The histone deacetylase SIRT6 regulates glucose homeostasis via Hif1α. *Cell* **2010,** 140, 280-293.

21. Sundaresan, N. R.; Vasudevan, P.; Zhong, L.; Kim, G.; Samant, S.; Parekh, V.;

Pillai, V. B.; Ravindra, P.; Gupta, M.; Jeevanandam, V. The sirtuin SIRT6 blocks IGF-Akt signaling and development of cardiac hypertrophy by targeting c-Jun. *Nat. Med.* **2012,** 18, 1643-1650.

22. Cai, Y.; Yu, S.-S.; Chen, S.-R.; Pi, R.-B.; Gao, S.; Li, H.; Ye, J.-T.; Liu, P.-Q. Nmnat2 protects cardiomyocytes from hypertrophy via activation of SIRT6. *FEBS Lett.* **2012,** 586, 866-874.

23. Min, L.; Ji, Y.; Bakiri, L.; Qiu, Z.; Cen, J.; Chen, X.; Chen, L.; Scheuch, H.; Zheng, H.; Qin, L. Liver cancer initiation is controlled by AP-1 through SIRT6-dependent inhibition of survivin. *Nat. Cell Biol.* **2012,** 14, 1203-1211.

24. Marquardt, J. U.; Fischer, K.; Baus, K.; Kashyap, A.; Ma, S.; Krupp, M.; Linke, M.; Teufel, A.; Zechner, U.; Strand, D. Sirtuin‐6–dependent genetic and epigenetic alterations are associated with poor clinical outcome in hepatocellular carcinoma patients. *Hepatology* **2013,** 58, 1054-1064.

25. Cagnetta, A.; Soncini, D.; Orecchioni, S.; Talarico, G.; Minetto, P.; Guolo, F.; Retali, V.; Colombo, N.; Carminati, E.; Clavio, M. Depletion of SIRT6 enzymatic activity increases acute myeloid leukemia cells' vulnerability to DNA-damaging agents. *Haematologica* **2018,** 103, 80-90.

26. Cea, M.; Cagnetta, A.; Adamia, S.; Acharya, C.; Tai, Y.-T.; Fulciniti, M.; Ohguchi, H.; Munshi, A.; Acharya, P.; Bhasin, M. K. Evidence for a role of the histone deacetylase SIRT6 in DNA damage response of multiple myeloma cells. *Blood* **2016,** 127, 1138-1150.

27. Kugel, S.; Sebastián, C.; Fitamant, J.; Ross, K. N.; Saha, S. K.; Jain, E.; Gladden, A.; Arora, K. S.; Kato, Y.; Rivera, M. N. SIRT6 suppresses pancreatic cancer through control of Lin28b. *Cell* **2016,** 165, 1401-1415.

28. Bauer, I.; Grozio, A.; Lasiglié, D.; Basile, G.; Sturla, L.; Magnone, M.; Sociali, G.;

Soncini, D.; Caffa, I.; Poggi, A. The NAD+-dependent histone deacetylase SIRT6 promotes cytokine production and migration in pancreatic cancer cells by regulating Ca^{2+} responses. *J. Biol. Chem.* **2012,** 287, 40924-40937.

29. Bhardwaj, A.; Das, S. SIRT6 deacetylates PKM2 to suppress its nuclear localization and oncogenic functions. *Proc. Natl. Acad. Sci.* **2016,** 113, E538-E547.

30. Ghosh, S.; Liu, B.; Wang, Y.; Hao, Q.; Zhou, Z. Lamin A is an endogenous SIRT6 activator and promotes SIRT6-mediated DNA repair. *Cell Rep.* **2015,** 13, 1396-1406.

31. You, W.; Rotili, D.; Li, T. M.; Kambach, C.; Meleshin, M.; Schutkowski, M.; Chua, K. F.; Mai, A.; Steegborn, C. Structural basis of sirtuin 6 activation by synthetic small molecules. *Angew. Chem. Int. Ed.* **2017,** 56, 1007-1011.

32. You, W.; Zheng, W.; Weiss, S.; Chua, K. F.; Steegborn, C. Structural basis for the activation and inhibition of Sirtuin 6 by quercetin and its derivatives. *Sci. Rep.* **2019**, 9, 1-11.

33. Huang, Z.; Zhao, J.; Deng, W.; Chen, Y.; Shang, J.; Song, K.; Zhang, L.; Wang, C.; Lu, S.; Yang, X. Identification of a cellularly active SIRT6 allosteric activator. *Nat. Chem. Biol.* **2018,** 14, 1118-1126.

34. Jones, G.; Willett, P.; Glen, R. C.; Leach, A. R.; Taylor, R. Development and validation of a genetic algorithm for flexible docking. *J. Mol. Biol.* **1997,** 267, 727-748.

35. Li, G.-B.; Yang, L.-L.; Wang, W.-J.; Li, L.-L.; Yang, S.-Y. ID-Score: a new empirical scoring function based on a comprehensive set of descriptors related to protein–ligand interactions. *J. Chem. Inf. Model.* **2013,** 53, 592-600.

36. Houston, D. R.; Walkinshaw, M. D. Consensus docking: improving the reliability of docking in a virtual screening context. *J. Chem. Inf. Model.* **2013,** 53, 384-390.

37. Huang, S.; Wang, X.; Lin, G.; Cheng, J.; Chen, X.; Sun, W.; Xiang, R.; Yu, Y.; Li,

L.; Yang, S. Discovery of human TyrRS inhibitors by structure-based virtual screening, structural optimization, and bioassays. *RSC Adv.* **2019,** 9, 9323-9330.

38. Huang, S.; Song, C.; Wang, X.; Zhang, G.; Wang, Y.; Jiang, X.; Sun, Q.; Huang, L.; Xiang, R.; Hu, Y. Discovery of new SIRT2 inhibitors by utilizing a consensus docking/scoring strategy and structure–activity relationship analysis. *J. Chem. Inf. Model.* **2017,** 57, 669-679.

39. Hu, J.; He, B.; Bhargava, S.; Lin, H. A fluorogenic assay for screening Sirt6 modulators. *Org. Biomol. Chem.* **2013,** 11, 5213-5216.

40. Milne, J. C.; Lambert, P. D.; Schenk, S.; Carney, D. P.; Smith, J. J.; Gagne, D. J.; Jin, L.; Boss, O.; Perni, R. B.; Vu, C. B. Small molecule activators of SIRT1 as therapeutics for the treatment of type 2 diabetes. *Nature* **2007,** 450, 712-716.

41. Davoren, J. E.; Nason, D.; Coe, J.; Dlugolenski, K.; Helal, C.; Harris, A. R.; LaChapelle, E.; Liang, S.; Liu, Y.; O'Connor, R. Discovery and lead optimization of atropisomer D1 agonists with reduced desensitization. *J. Med. Chem.* **2018,** 61, 11384-11397.

42. Kim, H.-S.; Xiao, C.; Wang, R.-H.; Lahusen, T.; Xu, X.; Vassilopoulos, A.; Vazquez-Ortiz, G.; Jeong, W.-I.; Park, O.; Ki, S. H. Hepatic-specific disruption of SIRT6 in mice results in fatty liver formation due to enhanced glycolysis and triglyceride synthesis. *Cell Metab.* **2010,** 12, 224-236.

43. Kokkonen, P.; Rahnasto-Rilla, M.; Mellini, P.; Jarho, E.; Lahtela-Kakkonen, M.; Kokkola, T. Studying SIRT6 regulation using H3K56 based substrate and small molecules. *Eur. J. Pharm. Sci.* **2014,** 63, 71-76.

44. Niesen, F. H.; Berglund, H.; Vedadi, M. The use of differential scanning fluorimetry to detect ligand interactions that promote protein stability. *Nat. Protoc.* **2007,** 2, 2212-2221.

45. Verdonk, M. L.; Chessari, G.; Cole, J. C.; Hartshorn, M. J.; Murray, C. W.; Nissink, J. W. M.; Taylor, R. D.; Taylor, R. Modeling water molecules in protein−ligand docking using GOLD. *J. Med. Chem.* **2005,** 48, 6504-6515.

46. Olson, M. E.; Abate-Pella, D.; Perkins, A. L.; Li, M.; Carpenter, M. A.; Rathore, A.; Harris, R. S.; Harki, D. A. Oxidative reactivities of 2-furylquinolines: ubiquitous scaffolds in common high-throughput screening libraries. *J. Med. Chem.* **2015,** 58, 7419-7430.

47. Dahal, U. P.; Joswig-Jones, C.; Jones, J. P. Comparative study of the affinity and metabolism of type I and type II binding quinoline carboxamide analogues by cytochrome P450 3A4. *J. Med. Chem.* **2011,** 55, 280-290.

48. Spinks, D.; Shanks, E. J.; Cleghorn, L. A.; McElroy, S.; Jones, D.; James, D.; Fairlamb, A. H.; Frearson, J. A.; Wyatt, P. G.; Gilbert, I. H. Investigation of trypanothione reductase as a drug target in Trypanosoma brucei. *ChemMedChem* **2009,** 4, 2060-2069.

49. Zhu, L.; Luo, K.; Li, K.; Jin, Y.; Lin, J. Design, synthesis and biological evaluation of 2-phenylquinoline-4-carboxamide derivatives as a new class of tubulin polymerization inhibitors. *Bioorg. Med. Chem.* **2017,** 25, 5939-5951.

50. Chen, X.; Peng, W.; Huang, S.; Yang, C.; Hu, M.; Yang, S.; Yang, S.; Xie, Y.; Chen, H.; Lei, N. Novel mitochondria-targeted and fluorescent DNA alkylation agents with highly selective activity against cancer cells. *Dyes Pigm.* **2019**, 107610.

51. Krzyzosiak, A.; Sigurdardottir, A.; Luh, L.; Carrara, M.; Das, I.; Schneider, K.; Bertolotti, A. Target-based discovery of an inhibitor of the regulatory phosphatase PPP1R15B. *Cell* **2018,** 174, 1216-1228. e19.

52. Banerjee, M.; Poddar, A.; Mitra, G.; Surolia, A.; Owa, T.; Bhattacharyya, B. Sulfonamide drugs binding to the colchicine site of tubulin: thermodynamic analysis

of the drug− tubulin interactions by isothermal titration calorimetry. *J. Med. Chem.* **2005,** 48, 547-555.

53. Schnapp, G.; Klein, T.; Hoevels, Y.; Bakker, R. A.; Nar, H. Comparative analysis of binding kinetics and thermodynamics of dipeptidyl peptidase-4 inhibitors and their relationship to structure. *J. Med. Chem.* **2016,** 59, 7466-7477.

54. Chen, X.; Chen, H.; Lu, C.; Yang, C.; Yu, X.; Li, K.; Xie, Y. Novel mitochondria-targeted, nitrogen mustard-based DNA alkylation agents with near infrared fluorescence emission. *Talanta* **2016,** 161, 888-893.

55. Pan, Y.; Zheng, M.; Zhong, L.; Yang, J.; Zhou, S.; Qin, Y.; Xiang, R.; Chen, Y.; Yang, S.-Y. A preclinical evaluation of SKLB261, a multikinase inhibitor of EGFR/Src/VEGFR2, as a therapeutic agent against pancreatic cancer. *Mol. Cancer Ther.* **2015,** 14, 407-418.

56. Zheng, M.-W.; Zhang, C.-H.; Chen, K.; Huang, M.; Li, Y.-P.; Lin, W.-T.; Zhang, R.-J.; Zhong, L.; Xiang, R.; Li, L.-L. Preclinical evaluation of a novel orally available SRC/Raf/VEGFR2 inhibitor, SKLB646, in the treatment of triple-negative breast cancer. *Mol. Cancer Ther.* **2016,** 15, 366-378.

Table of Contents Graphic